JOURNAL OF GEOPHYSICAL RESEARCH, VOL. 106, NO. B5, PAGES 8665-8686, MAY 10, 2001

Pervasive pressure solution transfer in a quartz sand

A. Revil

Centre National de la Recherche Scientifique, Centre Européen de Recherche et d'Enseignement en Géosciences de l'Environnement, Department of Geophysics, Aix-en-Provence, France

Abstract. The kinetics of deformation of a quartz aggregate by pervasive pressure solution can be, under certain conditions of temperature and grain size, strongly dependent upon the diffusivity of silica into the grain-to-grain contacts. An analysis of the factors affecting this key parameter (and less well constrained in the analysis of the problem of rock deformation by pressure solution) is presented. This analysis is based on recent advances on studying silica surfaces and particularly on the existence of a silica gel layer on the silica surfaces undergoing dissolution. By reinvestigating the electroviscous effect occurring at the grain-to-grain contact the present analysis shows that the diffusivity of silica at the grain-to-grain contacts is likely to be relatively similar to that in the bulk pore water (maybe 1 order of magnitude smaller but not more). This contradicts the previous work by *Rutter* [1976], which has been the key reference used in many subsequent papers to justify an extremely low value for the diffusivity of silica at the grain-to-grain contacts (5 orders of magnitude smaller than the diffusivity of silica in free water). This finding has dramatic implications concerning the deformation rate of quartz sands and sandstones by pressure solution in sedimentary basins with regard to (1) the limiting step affecting the kinetics of the process (diffusion of the solute or dissolution/precipitation chemistry) and (2) the existence of a thermodynamic equilibrium state when deformation by pressure solution occurs over geological timescales. A poroviscoplastic model is used to describe deformation associated with pervasive pressure solution transfer in quartz sands. This model is shown to be consistent with the current state of knowledge of the surface chemistry of silica. In addition, the comparison between this model and both laboratory and field data is rather good.

1. Introduction

A stressed quartz sand saturated with water deforms pervasively by matter transport through the water phase. An excess of dissolved silica, $Si(OH)_4$, is produced by the stress-enhanced dissolution of the grain-to-grain contacts. This excess of dissolved silica migrates by diffusion inside these grain-to-grain contacts and from the grain-to-grain contacts into the surrounding pore space. Oversaturation of the bulk pore water in silica leads to the precipitation of the solute as euhedral quartz overgrowths on the free surfaces of the grains [e.g., *Rutter*, 1976; *Houseknecht*, 1988; *Palciauskas and Domenico*, 1989; *Wahab*, 1998]. This phenomenon is called "pervasive pressure solution transfer" (PPST). It is one of the main deformation mechanism occurring in the upper crust of our planet [e.g., *Gratier and Gamond*, 1990; *Gratier*, 1993]. Pervasive pressure solution is also an important deformation mechanism in sedimentary basins at depth below ~2 km [*Maxwell*, 1964; *Houseknecht*, 1988; *Palciauskas and Domenico*, 1989; *Fowler and Yang*, 1999; *Yang*, 2000] as well as in active faults [*Sleep and Blanpied*, 1992, 1994; *Sleep*, 1994; *Segall and Rice*, 1995; *Bos et al.*, 2000; *Kanagawa et al.*, 2000]. This explains the high interest of geoscientists in this deformation mechanism, which has been studied since the end of the last century [*Sorby*, 1863, 1908].

The first part of this paper is focused on the study of the diffusivity of silica at the grain-to-grain contacts during deformation by PPST. During the last 24 years, the paper by *Rutter* [1976] has been a key reference for research scientists working to understand deformation by pressure solution in quartz sands. Rutter mentioned in his paper that the diffusivity of silica at the grain-to-grain contacts, a key variable in the study of PPST, is probably 5 orders of magnitude smaller than in the bulk water. *Rutter* [1976] justified this extremely low value as a result of the so-called "electroviscous effect". However, there are two electroviscous effects described in colloidal chemistry and only one of them is relevant to the situation occurring at the grain-to-grain contacts during deformation by PPST. *Rutter* [1976, 1978] cautioned that neither the silica diffusivity nor the effective thickness of the diffusion pathways at the grain-to-grain contacts is known with any precision. However, in papers published after 1976 and related to pressure solution [e.g., *Angevine and Turcotte*, 1983; *Tada et al.*, 1987; *Mullis*, 1991; *Lemée and Gueguen*, 1996], most of the research scientists used the diffusivity value proposed by Rutter without questioning its validity and the foundations of the electroviscous phenomenon mentionned by Rutter to justify an extremely low value for the silica diffusivity at the grain-to-grain contacts. In this paper, the problem of the diffusivity of silica at the grain-to-grain contacts is reexamined to the light of modern electrochemistry. Very different conclusions are reached below concerning this key parameter.

In addition, the value of the silica diffusivity at the grain-to-grain contacts has implications concerning the rheology describing deformation by pressure solution. Two main types of rheological models have been used in the past to describe deformation of porous aggregates by pressure solution. In a first set of papers, a Newtonian rheological law was used to

Paper number 2000JB900465.
0148-0227/01/2000JB900465$09.00

interpret laboratory measurements [e.g., *Weyl*, 1959; *Rutter*, 1976; *Dewers and Ortoleva*, 1990, *Mullis*, 1991]. The application of this Newtonian rheological law to field data (particularly to compaction pathways of clean sandstones in sedimentary basins over geological timescales) requires a very low value for the silica diffusivity at the grain-to-grain contacts [e.g., *Angevine and Turcotte*, 1983]. In a second set of papers, *Palciauskas and Domenico* [1989] and *Stephenson et al.* [1992] contested the Newtonian rheological law as describing PPST over geological timescales. They used instead a purely plastic law to interpret "equilibrium" compaction phenomena related to PPST in sedimentary basins. The term "plastic" can be misleading as this term is used in the literature with very different meanings (e.g., it is sometimes used as synonymous of "intragranular deformation" or with a purely rheological meaning without any description of the microscopic processes responsible for the macroscopic deformation). The term "plastic" is used below to describe a dissipative, irreversible process in which time does not appear explicitly in the constitutive equations.

In a preliminary work, *Revil* [1999] developed a new model incorporating the two previous modeling attempts (Newtonian and plastic) inside a unified approach. He used a Voigt-type viscoplastic rheological model to describe the bulk deformation associated with pervasive pressure solution transfer. In his model, viscous compaction describes the kinetics of rock deformation by pressure solution, whereas the plastic limit corresponds to a thermodynamic (compaction) equilibrium state (exactly in the same way we consider separately the kinetics and the final thermodynamic equilibrium state of a chemical reaction). However, this point of view was not yet supported by some explanations at the molecular scales. It could be argued that once stressed, there is always a finite chemical potential gradient at the grain-to-grain contacts that drives the solute transfer. In such a case, this would lead to steading state diffusion creep by opposition to compaction equilibrium. We provide below a number of arguments to support the rheological model proposed by *Revil* [1999]. These arguments are consistent with our state of knowledge of silica chemistry and the framework used to discuss silica diffusivity associated with PPST.

Section 2 of this paper contains a description of chemical, mechanical, and thermodynamic equilibria at a stressed grain-to-grain contact during PPST. In section 3 the diffusivity of silica is shown to be very similar to that measured in the bulk water (or at least one order of magnitude smaller, not more). It is also shown that the assumption of the electroviscous effect to justify an extremely small silica diffusivity at the grain-to-grain contacts can be ruled out. In section 4, the bulk deformation associated with PPST is described by a poroviscoplastic rheological law, which is consistent with the results found in sections 2 and 3. Section 5 contains a comparison between this rheological model and a set of experimental data from the literature. In section 6 the model is applied to the compaction path of a clean sandstone in a sedimentary basin. Section 7 summarizes the concluding statements made in this work.

2. Description of the Grain-to-Grain Contacts

2.1. Basic Assumptions

I consider a representative elementary volume of a granular aggregate formed by a framework of well-sorted quartz grains saturated by distilled water or an aqueous electrolyte. A reference state is defined for pressure solution in which (1) no effective stress has been applied to the representative elementary volume prior to $t = 0$ (where t is time) and (2) the contiguity between the grains (defined by the ratio of the grain-to-grain contact area per grain to the surface area of the grain; see Figure 1 and *Takei* [1998]) is small (only pseudo-Hertzian contacts). The porosity in the reference state is written ϕ_0. The grains are assumed to have all the same size. In such a granular porous material the bulk effective stress is usually defined by [*Skempton*, 1960; *Bear and Bachmat*, 1990]

$$\sigma_{eff} = \sigma - (1-\varphi)p, \tag{1}$$

where φ is the (dimensionless) grain-to-grain contiguity (Figure 1), $(1-\varphi)$ is the wetness of the grains [*Takei*, 1998], σ is the confining pressure (in Pa) (i.e., $\sigma = \mathrm{Tr}(\overline{\sigma})/3$, where $\overline{\sigma}$ is the total stress tensor, $\mathrm{Tr}(\,.\,)$ is the trace of this tensor), and p (in Pa) is the pore fluid pressure (compressive stress are positive according to the rock mechanics convention).

Equation (1) assumes that the grain-to-grain contacts are dry. However, I will assume below that the grain-to-grain contacts of the compacting quartz aggregate are entirely wetted (see section 2.2). The water contained inside these grain-to-grain contacts is assumed to be at the same fluid pressure than the bulk pore water contained in the connected porosity. Therefore the effective stress felt by the grains is defined by

$$\sigma_{eff} = \sigma - p = (1-\phi)\sigma^S_{eff}, \tag{2}$$

$$\sigma^S_{eff} \equiv \sigma_S - p, \tag{3}$$

where σ_S is the average stress inside the grains, σ^S_{eff} is the average stress inside the grains above the pore fluid pressure, and $\sigma = \phi p + (1-\phi)\sigma_S$ is the phase average stress [*Palciauskas and Domenico*, 1989; *Takei*, 1998]. In such a situation, σ_{eff} is usually called the differential or "effective" stress. In sections 2 and 3, I will also assume that the effective stress history applied to the representative elementary volume is given by

$$\sigma_{eff}(t) = \mathrm{H}(t)\sigma_{eff}, \tag{4}$$

where the effective stress σ_{eff} is given by (2), σ and p are both independent of time, and $\mathrm{H}(t)$ is the Heaviside step function ($\mathrm{H}(t) = 0$ as $t < 0$ and $\mathrm{H}(t) = 1$ as $t \geq 0$), $t = 0$ is the time reference corresponding to the reference state discussed above. This assumption, typical of the so-called creep experiments, will be relaxed in section 4. Porosity and contiguity are the two key state-variables used in the problem of pressure solution. I note that ϕ_∞ and φ_∞ are the porosity and the contiguity at $t \to \infty$, whereas ϕ_0 and φ_0 correspond to the porosity and the contiguity at $t = 0^+$ (i.e., immediately after the application of the effective stress σ_{eff}).

2.2. Explanation for Open Diffusion Pathways

Once the bulk effective stress σ_{eff} is applied to the granular porous aggregate, PPST starts to be active. This chemical deformation process includes (1) dissolution of the grain-to-grain contacts, (2) diffusion of the solute inside the wetted grain-to-grain contacts, and (3) precipitation of the solute on the free grain surfaces due to silica oversaturation in the bulk pore water (Figure 1). The first step is due to a stress-enhanced solubility of the mineral at the grain-to-grain contacts by

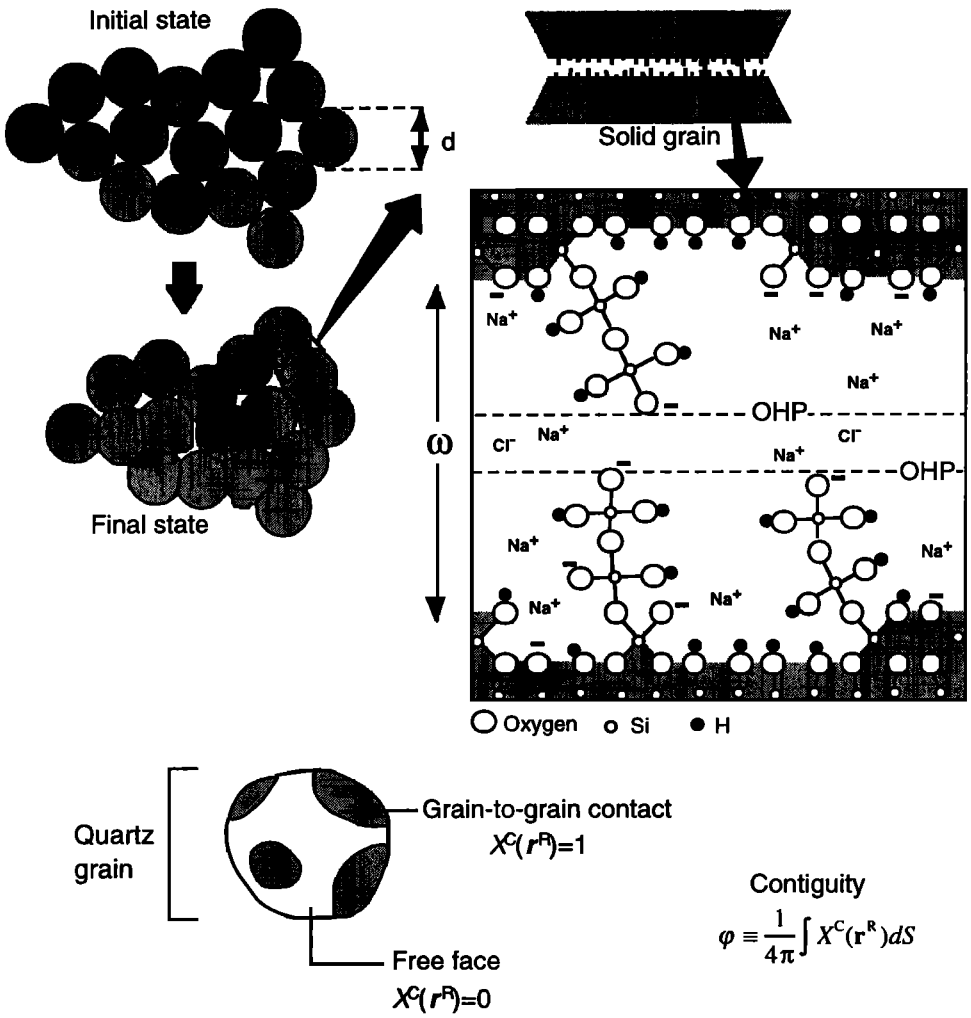

Figure 1. Pressure solution in clay-free quartz sands. We consider a representative elementary volume (REV) of a clay-free sand saturated by an aqueous solution and submitted to a given effective stress. Pressure solution starts by dissolution of the grain contacts, diffusion of the solute at the grain contacts, and precipitation on the free pore faces of the grains. This process increases the grain-to-grain contiguity and therefore decreases the stress concentration at the grain-to-grain contacts. The grain to grain contact area is formed by a gel layer of polysilicic acid chains, which result from dissolution of the grain-to-grain contacts. These chains form a brush of protruding "hairs," which can resist to high stress concentrations due to short-range steric repulsion. OHP is the outer Helmoltz plane. The contiguity of a grain is related to a contact function $X(\mathbf{r}^R)$ defined by $X(\mathbf{r}^R) = 1$ if the grain contacts with another grain at $\mathbf{r}^R$ and $X(\mathbf{r}^R) = 0$ otherwise [see *Takei*, 1998], $dS = \sin\theta\, d\theta\, d\psi$ where $(\theta, \psi, \mathbf{r})$ defines a spherical coordinate system for a spherical grain of radius R.

comparison with that on the free faces (see section 2.4). Indeed, as indicated in section 2.1, the effective stress σ_{eff} is only an average stress over the porous aggregate. Actually, there is a strong enhancement of the stress level at the grain-to-grain contacts especially at the beginning of the deformation process when the contiguity between the grains is small. PPST can be seen as a compactional response of the porous aggregate, which by increasing the surface area of the grain-to-grain contacts decreases the stress level at the grain-to-grain contacts down to a certain critical value in an attempts to reestablish a thermodynamic equilibrium state. Indeed, the kinetics step of this process of dissolution/precipitation holds until the solubility at these contacts, which depends on the local effective normal stress, is equal to the solubility on the free faces of the grains. Such a final thermodynamic equilibrium state is discussed further below in section 3.

One of the main critical question arising in the description of the process of PPST is about the existence of open diffusion pathways at the grain-to-grain contacts. Two assumptions have been made in the past to explain the existence of these diffusion pathways. They are (1) the "anomalous" properties of water in the vicinity of the mineral surface [e.g., *Weyl*, 1959; *Rutter*, 1976], and (2) the existence of a time statistically stable island structure [e.g., *Lehner and Bataille*, 1984].

Let us first discuss assumption 1. *Weyl* [1959] (followed by many authors) proposed that a thin continuous water film is preserved at the grain-to-grain contacts in the compacting quartz aggregate. To avoid to be squeezed out, this water film was assumed to support shear stresses. So it was believed that the water contained inside the grain-to-grain contacts is strongly adsorbed to the silica surface over tens of nanometers (several micrometers were sometimes advanced as plausible by some research scientists). It was also assumed that this strongly bound water is responsible for a hydration force, which was assumed to be repulsive. In a recent review paper, *Israelachvili and Wennerström* [1996] have shown that any

interactions that may arise from water structuring effects in the close vicinity of a silica/water interface are expected to be monotonically attractive or oscillatory with a periodicity of the diameter of the water molecule (0.25 nm), not repulsive. A similar conclusion was reached very recently by *Yaminsky et al.* [1998] but challenged by *Colic et al.* [1998] for perfectly planar interfaces. If confirmed, the explanation proposed by *Israelachvili and Wennerström* [1996] would rule out assumption 1 to explain open diffusive pathways at the grain-to-grain contacts in a compacting quartz sand. Actually, recent direct measurements of the viscosity of water and electrolyte solutions adjacent to silica surfaces have shown that the nonslip plane separating fixed and mobile water is located no further than one water layer from the mineral-water interface, which is again consistent with the absence of water structuring in the close vicinity of this interface except in the first hydration layer [see *Israelachvili and Wennerström*, 1996, and references therein]. *Horn et al.* [1989] have measured the viscosity of the pore fluid trapped between silica sheets and found a value equal to that found in the bulk pore water ($\sim 10^{-3}$ Pa s).

Lehner and Bataille [1984] proposed the existence of time-statistically stable ridge island structures at the grain-to-grain contacts, which would maintain some open pathways for diffusion of the solute. Such a structure was indeed observed in PPST associated with deformation of halite by *Spiers et al.* [1990] and *Hickman and Evans* [1995]. *Cox and Paterson* [1991] observed a network of islands and channels within the grain-to-grain contacts during an experiment performed on a fine powder of quartz grains at 1200 K. With such an assumption, *Ghoussoub* [2000] proposed a two-step evolution of the structure of the stressed grain-to-grain contacts. The first one consists of a diffusive morphology evolution in time and results in an enhancement of the initial stress concentrations inside the dry grain-to-grain contacts. The second step is characterized by a rapid and localized dissolution in the regions of stress concentrations. The localized dissolution provides a mechanism for the pore fluid to invade a previously solid-solid contact regions by marginal dissolution of the boundaries of these regions. She found that the newly wetted contact area is unstable pointing out a possible dynamic repeated reorganization of the grain-to-grain contact structure during deformation of the aggregate by pressure solution. The presence of such a time-statistically-stable island structure at the grain-to-grain contacts is not in contradiction with the model developed below. However, in such a case the effective grain-to-grain contiguity should be corrected for the true contact area between the grains.

We propose in this paper a third possibility to explain the existence of efficient diffusion pathways at the grain-to-grain contacts in compacting quartz aggregates. Still challenging nowadays, the electrochemical properties of the silica-water interface exhibit unique properties by comparison with other oxides and minerals [e.g., *Yates and Healy*, 1976; *Iler*, 1979; *Michael and Williams*, 1984; *Vigil et al.*, 1994]. Indeed, in certain conditions, like at high pH values for which the silica surface starts to dissolve, the density of silanol groups >Si-OH at the quartz/water interface can be higher than 25 sites nm^{-2}. This is much greater than the possible site density for a monolayer of silanol sites located on a flat surface ($\sim 6 \pm 4$ sites nm^{-2}) like usually found for other oxides. Hence, in such a case the silanol sites are located in a three-dimensional structure, which is actually a gel layer of hydrolyzed silica material resulting from the dissolution of the true mineral surface [e.g., *Iler*, 1979; *Vigil et al.*, 1994; *Israelachvili and Wennerström*, 1996]. This finding was shown to be consistent with experimental data obtained from surface force apparatus (SFA) techniques between two silica surfaces [e.g., *Vigil et al.*, 1994; *Israelachvili and Wennerström*, 1996]. Note that no other minerals exhibit such a behavior, which could point out a fundamental difference between PPST associated with silica and other minerals like halite often used in laboratory experiments.

A gel layer could develop at the grain-to-grain contacts of a compacting quartz aggregate undergoing dissolution. In other words, dissolution of silica at the grain-to-grain contacts would lead to the presence of an ~1 to 2 nm-thick gel layer at each silica water interface inside the grain contacts (as shown in Figure 1). These gel layers are formed by a three dimensional network of protruding polysilicic acid groups >Si-[O-Si(OH)$_2$]$_n$-OH (where > refers to the mineral crystalline network and n is the number of monomers present in the chain) as suggested by the experiments done by *Vigil et al.* [1994]. It was proposed by *Revil* [1999] that this gel layer is responsible for the anomalous properties of the fluid at the grain-to-grain contacts during pervasive pressure solution transfer in quartz aggregates and could provide efficient pathways for the diffusion of the solute resulting from the stress enhanced dissolution of the grain-to-grain contacts. Indeed, this gel layer is responsible for a polymer-like steric repulsion. This steric repulsion force is an exponentially repulsive force strong enough, at short contact distances (~ 2 nm, i.e., at distance corresponding to the dimensions of the protruding hairs), to overcome the attractive Van der Waals force, which otherwise would cause adhesion on contact [see *Vigil et al.*, 1994]. Similar monotonic repulsion forces have been measured recently between lipid bilayers and in various colloidal systems [e.g., *Vigil et al.*, 1994; *Israelachvili and Wennerström*, 1996; *Abraham et al.*, 2000; *Ennis et al.*, 2000, and references therein]. In the pH range 5-9, the silanol groups >Si-OH of the polysilicic acid hairs are charged through the following chemical reactions [e.g., *Revil et al.*, 1999a]:

$$> \mathrm{SiOH} \Leftrightarrow > \mathrm{SiO^-} + \mathrm{H^+} \quad (5)$$

$$> \mathrm{SiOH} + \mathrm{Me^+} \Leftrightarrow > \mathrm{Si(O^-Me^+)}, \quad (6)$$

where Me^+ is the metal cation resulting from the salt dissociation (e.g., Na^+ for NaCl). The surface charge due to the previous ion exchanges between the surface sites and the pore electrolyte is responsible for a long-range electrical field. The fixed surface charge resulting from (5) and (6) is counterbalanced by a cloud of "counterions" forming the so-called electrical diffuse layer (e.g., *Revil et al.* [1999a and references therein] and Figure 2). The fixed charge layer and the diffuse layer form the so-called electrical double (or triple) layer. The existence of open diffusion pathways is therefore a consequence of the interplay of all the forces acting at the grain-to-grain contacts including the steric repulsive force mentionned above, which is evaluated in section 2.3.

2.3. Mechanical Equilibrium

According to the situation described in section 2.3 the interactions between two silica surfaces at a grain-to-grain contact undergoing dissolution need to be considered in terms of the attractive Van der Waals and repulsive electrostatic

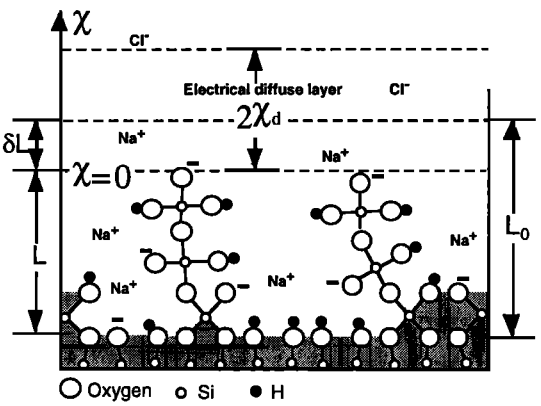

Figure 2. The effective pressure at a grain-to-grain contact calculated in a Lagrangian framework attached to the head of the polysilicic brush. The lengths L_0 and L are the initial (unstressed) and confined thicknesses of the protruding layer, respectively, and χ_d is the Debye length.

pressures and an additional polymer-like steric repulsion pressure having a short-range interaction. Note that recent theoretical developments [e.g., *Ninham and Yaminski*, 1997] seems to show that a decomposition between Van der Waals and electrical double-layer forces may not be strictly valid. However, we will assume below that such decomposition remains a good approximation. The reference state for the mechanical behavior of a grain-to-grain contact is defined with the two silica surfaces at infinity, and we consider a framework attached to the edge of the polysilicic polymeric brushes (Figure 2). Therefore this framework follows the top of the brush during its compression in response to the action of the confining stress applied over the representative elementary volume at $t > 0$. The normal traction at the grain-to-grain contact has to be continuous. Therefore when two grains are brought in close interaction to each other (Figure 3), the mechanical equilibrium at the grain-to-grain contacts is

$$\sigma_n(\varphi) - p + \Pi_V(\omega) - \Pi_e(\omega) - \Pi_S(\omega) + 2\gamma H = 0, \qquad (7)$$

where γ is the surface tension (Gibbs's surface free energy, ~0.5 J m^{-2} [see *Parks*, 1984 and *Heidug* 1995]), H denotes the mean local curvature (in m^{-1}) of the pore fluid-grain interface, which is related to the two principal curvature radii of the interface r_1 and r_2 by $H = 2\,(1/r_1 + 1/r_2)$ (H is positive when the grain is bounded by a concave surface [*Heidug*, 1995]), σ_n represents the local normal compressive pressure acting on each grain normal to the common tangent plane at the surface of contact, ω is the distance between the two silica surfaces at the grain-to-grain contacts (Figure 1), Π_V represents the Van der Waals (attractive) pressure, Π_e represents the repulsive electrostatic pressure, and Π_S represents the (repulsive) steric pressure due to the confining of the two silica polymeric brushes (note that compressive pressure are taken positive below to be consistent with that used for the macroscopic effective stress; this convention is opposite to that usually used in colloidal chemistry). In the case where the confining pressure is too high, the two grain surfaces at the grain-to-grain contacts can collapse locally by sintering of the two surfaces (Figure 3). This would form some dry contacts asperities (i.e., direct solid-solid contacts) inside the grain-to-grain contacts. However, in such a case, pressure solution would be promoted at the margins of these solid-solid contacts by local stress concentrations and disjoining steric pressures in the way envisioned by *Tada et al.* [1987]. It follows that these dry contacts would disappeared quickly with time.

The normal compressive pressure at a grain-to-grain contact is defined by [e.g., *Heidug*, 1995]

$$\sigma_n = -\mathbf{n} \cdot \boldsymbol{\Sigma}\, \mathbf{n}, \qquad (8)$$

where $\mathbf{n}$ is the unit vector normal to the solid-fluid interface and oriented toward the fluid phase and $\boldsymbol{\Sigma}$ is the stress tensor in the solid when the surface forces are switched off at the grain-to-grain contacts (it is approximately equal to the Cauchy stress tensor in the grains, [see *Heidug*, 1995]). The relationship between the differential stress $\Delta\sigma_n \equiv \sigma_n - p$, the effective stress σ_{eff}, and the grain-to-grain contiguity is

$$\Delta\sigma_n = \frac{\sigma_{eff}\,\mathrm{H}(t)}{\varphi(t)}. \qquad (9)$$

The terms Π_V and Π_e correspond to the so-called DVLO forces [*Israelachvili* 1992; *Vigil et al.*, 1994], DVLO is an

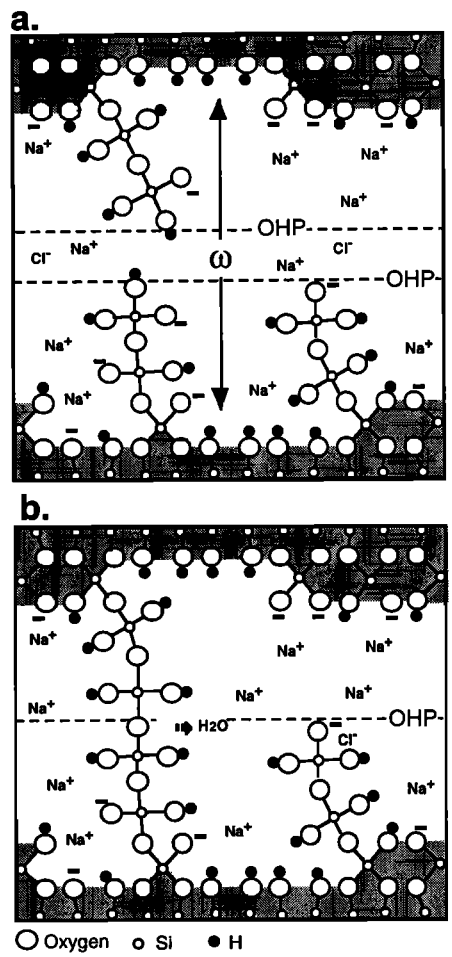

Figure 3. Interaction between two silica brushes when two grains are brought in close contact to each other. (a) Four forces interact at a stressed grain-to-grain contact including the Van der Waals, the electrostatic, the steric, and the mechanical forces. (b) Eventually, the open pathways can collapse by sintering of the two hydrophilic surfaces.

abbrevation for Derjaguin, Verwey, Landau, and Overbeek classical theory of force interaction between two surfaces). The Van der Waals and electrostatic pressures are given by a modified form of the DVLO theory [*Paunov and Binks*, 1999]

$$\Pi_V(\omega) \approx \frac{A}{6\pi(\omega - 2L)^3}, \quad (10)$$

$$\Pi_e(\omega) = 64 k_b T C_f \tanh^2\left(\frac{\tilde{\varphi}_0}{4}\right)\left[1 + 4\upsilon C_f \sinh^2\left(\frac{\tilde{\varphi}_0}{4}\right)\right] \times \exp\left(-\frac{\omega - 2L}{\chi_d}\right), \quad \omega - 2L \gg \chi_d, \quad (11)$$

$$\Pi_e(\omega) = \frac{k_b T}{\upsilon}\ln\left[1 + 4\upsilon C_f \sinh^2\left(\frac{\tilde{\varphi}_0}{2}\right)\right] - \frac{k_b T C_f}{2}\left(\frac{\omega - 2L}{\chi_d}\right) \times \frac{\sinh^2(\tilde{\varphi}_0)}{\left[1 + 4\upsilon C_f \sinh^2\left(\frac{\tilde{\varphi}_0}{2}\right)\right]}, \quad \omega - 2L < \frac{\chi_d}{3}, \quad (12)$$

$$\tilde{\varphi}_0 \equiv \frac{e\varphi_0}{k_b T}, \quad (13)$$

$$\chi_d \equiv \sqrt{\frac{\varepsilon_f k_b T}{2e^2 C_f}}, \quad (14)$$

where $\tanh x = (e^x - e^{-x}) / (e^x + e^{-x})$, $\sinh x = (e^x - e^{-x}) / 2$, χ_d (in m) is the Debye screening length, A is the nonretarded Hamaker's constant ($\approx 6 \times 10^{-20}$ J [see *Vigil et al.*, 1994]), C_f (in mol L^{-1}) is the salinity of the fluid at the grain-to-grain contacts, φ_0 (in V) is the electrostatic potential at the surface of the brush (i.e., at the outer Helmoltz plane as shown in Figure 1), ε_f is the dielectric constant of the fluid at the grain-to-grain contacts ($\varepsilon_f = 80\ \varepsilon_0$ with $\varepsilon_0 = 8.84 \times 10^{-12}$ F m^{-1}), e (>0) is the elementary charge (1.6×10^{-19} C), ω (in m) is the thickness of the diffusion pathways at the grain-to-grain contacts (including the thickness of the two polymeric brushes, see Figure 1), L is the thickness of the gel layer (in m), and υ (in m^3) has the sense of an excluded volume parameter approximately equal to 8 times the volume of the hydrated counterion (see *Paunov and Binks* [1999] and Table 1). Usually, the ionic strength of the pore water solution is dominated by the concentration of the salt, and in such a case the ionic strength is taken equal to the salinity. However, in most experiments, distilled water at pH ≈ 6 ± 1 is used, and in such a condition the salinity (or more precisely the ionic strength) is controlled by the solubility of the mineral.

Table 1. Hydrated Radius and Excluded Volume of Some Ions

Ion	Hydrated Radius,[a] nm	Excluded Volume,[b] nm³
Li^+	0.38	1.84
Na^+	0.36	1.56
K^+	0.33	1.20
Cs^+	0.33	1.20
Ca^{2+}	0.41	2.31
Al^{3+}	0.48	3.71
Cl^-	0.33	1.20

[a]From a compilation by *Israelachvili* [1992, p. 55].
[b]Eight times the hydrated volume.

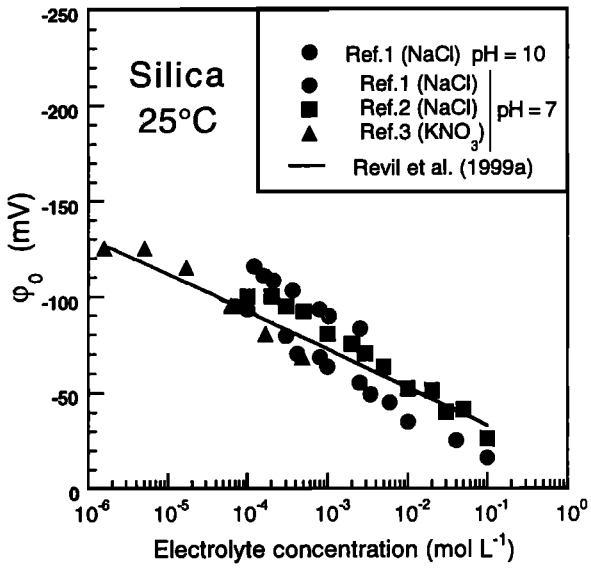

Figure 4. Surface electrical potential φ_0 (in mV) at the silica-water interface versus the brine salinity. We have assumed that the potential φ_0 is equal to the ζ potential determined from electrokinetic measurements [see *Revil et al.*, 1999a]. Reference 1, *Gaudin and Fuerstenau* [1955]; reference 2, *Li and de Bruyn* [1966]; reference 3, *Watillon and de Backer* [1970].

The potential φ_0 in (11) and (12) depends strongly on the pore water salinity (see Figure 4). At a first level of approximation, φ_0 can be equated to the so-called ζ potential, which can be determined by electrokinetic measurements [e.g., *Revil et al.*, 1999a, their Figure 4]. The relationship between the ζ potential and the salinity can be determined from a formula derived by *Revil et al.* [1999a]:

$$\varphi_0 = b\left(\log_{10} C_f\right) + c, \quad (15)$$

$$b \equiv \frac{k_b T}{3e}\ln 10, \quad (16)$$

$$c \equiv \frac{2k_b T}{3e}\ln\left(\frac{\sqrt{8 \times 10^3 \varepsilon_f k_b T N}}{2\, e \Gamma_S^0 K_{(-)}} 10^{-pH}\right), \quad (17)$$

where Γ_S^0 is the total surface site density of the mineral surface, $K_{(-)}$ is the equilibrium constant for the chemical reaction (3) (see *Revil et al.* [1999a] for some realistic values for both Γ_S^0 and $K_{(-)}$), and N is the Avogadro number. At 25°C, $b \approx 20$ mV per tenfold change in concentration C_f of a 1:1 monovalent electrolyte in good agreement with the experimental data reported by *Pride and Morgan* [1991] ($b = 24 \pm 4$ mV per molar decade) and *Wan* [1991] (b = 18 mV per molar decade). Combining equations (11) or (12) with equations (15)-(17) and using the values listed in Table 1 implies that the electrostatic pressure is few megapascals in strength and its value is very sensitive to the *p*H, the salinity, and to a lesser extent to the type of counterion (as υ is sensitive to the type and valence of the salt cation, see Table 1).

The fifth term of (7) corresponds to short-range thermal fluctuations (steric) and osmotic-type forces, which are very repulsive short-range forces acting when the two polymeric brushes are pushed in close interaction with each other (see *Pincus* [1991] for an extensive discussion of the interaction between charged and uncharged grafted polymeric brushes). Once two brush-bearing surfaces are closer than twice the initial thickness of the brush layer L_0, there is a strong repulsive pressure between them. An order of magnitude of this steric pressure is given by the Alexander - de Gennes relationship [e.g., *Israelachvili*, 1992, p. 295],

$$\Pi_S(\omega) \approx \frac{100 k_b T}{s^3} \exp\left(-\frac{\pi \omega}{L_0}\right), \tag{18}$$

as $0.2 \leq \omega / (2\ L_0) \leq 0.9$ and where s is the mean distance between the polysilicic hairs, which is related to the number of polymeric hair per unit area Γ (the grafting density of the polymeric hairs) by $\Gamma = 1 / s^2$ (≤ 1 nm^{-2}). The strength of the steric repulsive pressure is computed versus the normalized length $\omega / (2\ L_0)$ in Figure 5 (see Table 2). The steric force is not sensitive to pH and ionic strength of the pore fluid solution. Simple calculations on the orders of magnitude of the different pressure terms show that the electrostatic and Van der Waals forces can be safely neglected at short grain-to-grain contact distances by comparison with the steric repulsion force when the grafting density of the polysilicic hair is ~1 nm^{-2}. In addition, we neglect below the surface tension term by assuming that the thickness of the grain-to-grain contacts is very thin compared to the length scale associated with the local curvature of the grain water interface inside the grain-to-grain contacts. From (7) and (9), it follows that

$$\sigma_n(t) - p - \Pi_S(t) = 0, \tag{19}$$

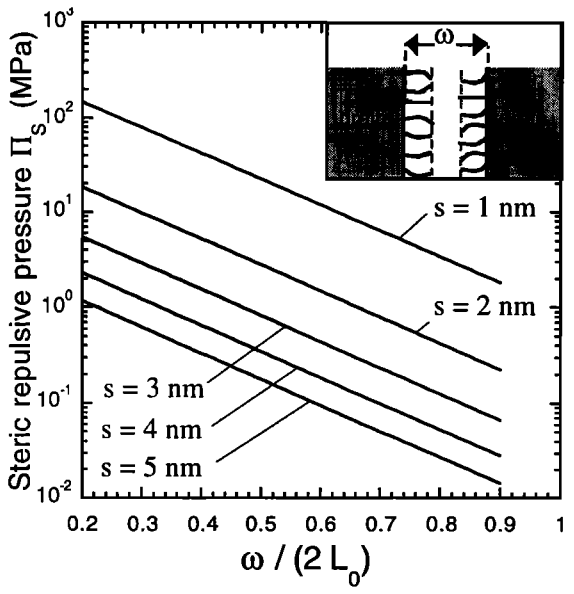

Figure 5. Intensity of the repulsive steric pressure (in MPa) versus the normalized grain-to-grain contact separation $\omega / (2\ L_0)$ where L_0 is the initial unconfined thickness of the polymeric gel layer. The calculations are made according to the Alexander-de Gennes theory, at 100°C and for various mean distances between the polymeric hairs s.

Table 2. Properties of the Gel Layer at the Grain-to-Grain Contacts

Parameter Meaning	Parameter Value
Number of monomer in the polymeric chain	n = 6
Initial thickness of the brush layer	L_0 = 3 nm
Final thickness of the brush layer	L = 1 nm
Mean distance between the polymeric hair	s = 1 nm
Computed steric pressure	Π_S = 63 MPa

$$\frac{\sigma_{eff} \mathrm{H}(t)}{\varphi(t)} = \Pi_S(t). \tag{20}$$

Therefore it follows that the repulsive steric pressure would adjust to maintain mechanical equilibrium at any stage of compaction of the porous aggregate. This can be achieve by a change of the thickness of the grain-to-grain contacts ω with time. We note φ_∞ the value of φ in the thermodynamic equilibrium state defined in section 2.4. In the thermodynamic equilibrium state, the contiguity is given by

$$\varphi_\infty = \frac{\sigma_{eff}}{\Pi_S(\infty)}. \tag{21}$$

In this section we have shown that the disjoining steric pressure controls the existence of wetted grain-to-grain contacts in a purely mechanical way. The evolution of the thickness of the diffusion pathways at the grain-to-grain contacts is determined by the requirement of mechanical equilibrium. In section 2.4 we examine the conditions of thermodynamic nonequilibrium and equilibrium states at the pore-fluid interface.

2.4. Kinetics and Equilibrium States

According to *Asaro and Tiller* [1977] and *Gal and Nur* [1998] the chemical potential of a surface element of a stressed grain at constant temperature can be written by

$$\mu_S = \mu_0 + w - \sigma_n \Omega + \gamma H \Omega, \tag{22}$$

where μ_0 is the chemical potential of the same grain surface element in the reference (unstressed) state, w is the molar strain energy (including elastic and inelastic components), σ_n is the normal component of the stress at the grain-to-grain contact (positive in compression), and Ω is the molecular volume of the solid phase, $\Omega = M_{SiO_2} / \rho_g$ ~3.77 x 10^{-29} m^3, ρ_g is the density of quartz (2650 kg m^{-3}), M_{SiO_2} is the molecular weight of quartz (60.08 x 10^{-3} kg mol^{-1}) (the change of the molecular volume with pressure is a second-order effect in conditions of pressure and temperature existing in sedimentary basins and this effect will be neglected below [*Kennedy*, 1950]). Assuming again that the thickness of the grain-to-grain contacts is small by comparison with the length scale associated with the curvature of the solid-water interface inside the grain-to-grain contacts, we neglect the surface energy term in (22). Therefore the chemical potential difference $\Delta \mu_S$ for the solute between a specific surface element of the stressed grain-to-grain contact compared with an element of surface of a free face of the same grain is given by

$$\Delta\mu_S = \Delta w - \Delta\sigma_n \Omega, \tag{23}$$

where Δw is the strain energy difference between the stressed grain-to-grain contacts and the free faces [e.g., *De Boer*, 1977] and $\Delta\sigma_n = \sigma_n - p$ is the normal stress difference between the grain-to-grain contact and the free faces of the grain ($\Delta\sigma_n = 0$ outside the grain-to-grain contact area).

The chemical potential difference driving pressure solution is related to the solubility by

$$\Delta\mu_S = \mu_0 - k_b T \ln\left(C_S\right) - \mu_0 + k_b T \ln\left(C_S^0\right), \tag{24}$$

$$\Delta\mu_S = k_b T \ln\left(C_S^0 / C_S\right), \tag{25}$$

where C_S^0 (in mol m^{-3}) is the concentration in aqueous silica in equilibrium with quartz grains at pore fluid pressure and temperature in hydrostatic pressure conditions whereas C_S is the concentration in aqueous silica with a normal stress at the grain-to-grain contacts above the state of hydrostatic pressure. Combining (23) and (25) yields

$$C_S = C_S^0 \exp\left[\frac{1}{k_b T}\left(\Omega\Delta\sigma_n - \Delta w\right)\right]. \tag{26}$$

Therefore there is a stress enhancement of the solubility only if $\Delta\sigma_n \geq \Delta w / \Omega$, i.e., only if the effective normal stress at the grain-to-grain contacts is higher than a critical level corresponding to the strain energy term. Equation (26) describes the kinetics of pressure solution transfer. This kinetics state describes the transient response of the compacting aggregate to the imposed effective stress until a thermodynamic equilibrium is reached. Thermodynamic equilibrium corresponds to the condition for which solute transfer stops between the stressed grain-to-grain contacts and the free faces of the grains. From (26) this condition yields

$$\Omega\Delta\sigma_n(\infty) = \Delta w(\infty). \tag{27}$$

We can now interpret this relationship in a more physical way. The expression $\Delta\sigma_n dV$ represents the molar displacement work done in displacing a volume dV of silica from the grain-to-grain contacts to the free grain faces. We shall assume that in the compaction equilibrium state this work is just equal to the energy per silica molecule required to activate plastic flow E_p times the number n of silica molecules displaced. This leads to $\Delta\sigma_n(\infty) = E_p\,(n / dV) = E_p / \Omega$ and therefore $\Delta w(\infty) = E_p$, i.e., the strain energy needed to displace silica in the equilibrium state is actually the molar energy needed to activate plastic flow.

The inverse of the grain-to-grain contiguity ($1/\varphi$) represents the stress enhancement factor between the macroscopic effective stress and the local normal stress at the grain-to-grain contacts. The use of (9) and (27) yields

$$\Delta\sigma_n(\infty) = \sigma_{eff} / \varphi_\infty, \tag{28}$$

$$\Delta w(\infty) = \Omega\sigma_{eff} / \varphi_\infty. \tag{29}$$

Note that $\Delta\sigma_n(\infty) = \Pi_S(\infty)$ according to the mechanical equilibrium state applied at $t \to \infty$. From (26), (28), and (29) the evolution with time of the solubility of the stressed grain contacts is given by

$$C_S(t) \approx C_S^0 \exp\left[\frac{\Omega}{k_b T \varphi_\infty}\left(\frac{\varphi_\infty}{\varphi(t)} - 1\right)\sigma_{\text{eff}} \mathrm{H}(t)\right], \tag{30}$$

$$\lim_{t\to\infty} C_S(t) = C_S^0, \tag{31}$$

which provides a new relationship between the mineral solubility at the grain-to-grain contacts and the grain-to-grain contiguity. A complete description of the evolution of the grain-to-grain contiguity as a function of time would require to specify the microgeometry of the porous aggregate. This is out of the scope of the present paper, and the evolution of this very important state variable as a function of the state of compaction of the compacting aggregate will be presented in a future paper.

A complete physical understanding of the time behavior of the stressed quartz aggregate is now possible (Figure 6). Let us assume that the effective stress history is given by (4). A grain can support only stresses up to a critical value before PPST starts to be active. Any further increase in the effective stress

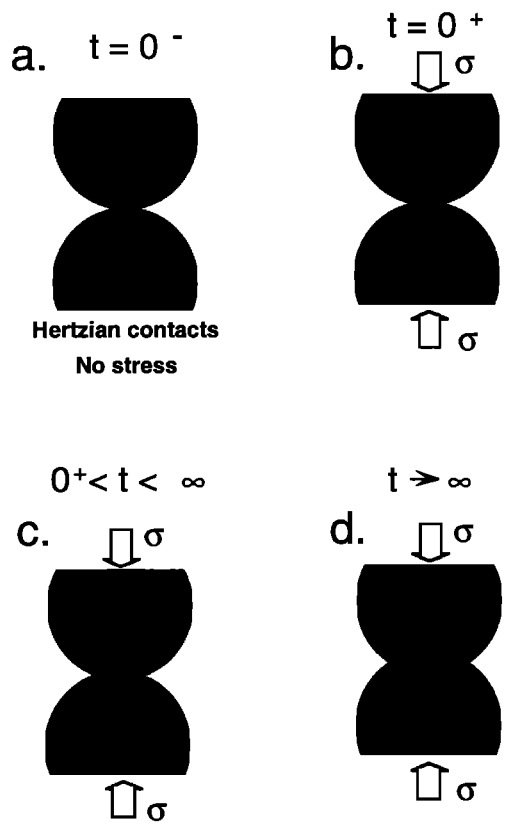

Figure 6. (a) In the reference state the grains assumed to be in contact through hertzian contacts. (b) Once stressed, a small grain-to-grain contiguity appears as the result of elastic deformation of the grains. At that stage, the normal effective stress at the grain-to-grain contacts is still very high. (c) Then dissolution/precipitation processes due to stress-enhanced solubility, which increases the grain-to-grain contiguity with time, so the stress at these contacts is redistributed over a larger grain-to-grain contact area decreasing the normal effective stress at these contacts with time. (d) The process which stops once the normal stress at the grain-to-grain contacts reaches a critical level discussed in the main text.

increases the microscopic stress level $\Delta\sigma_n$ at the grain-to-grain contacts above the stress critical value and results in pervasive pressure solution transfer in these contacts. PPST continues, increasing the grain-to-grain contiguity, until the critical value is reestablished at a larger contact area between the grains. If the time constant τ for this response is much shorter than the time scale of observation t(obs), the response will appear plastic. In the opposite case the response will appear viscous. A rheological law describing this process is presented in section 4.

3. Silica Diffusivity

Rutter [1976] argued that the diffusivity of silica inside the grain-to-grain contacts is 5 orders of magnitudes smaller than in the bulk pore water. He justified this extremely low value as a result of the electroviscous effect. The electroviscous effect describes the influence of the electrical field occurring inside the electrical double layer upon the dynamic shear viscosity of water in the vicinity of the mineral water interface (note that diffusivity and viscosity are related to each other by the Stokes-Einstein relationship). However, it appears that there is a fundamental misconception in the paper of Rutter about what is called the electroviscous effect and especially on how to compute its influence upon the solute diffusivity. This confusion arises because there are two electroviscous effects described in the literature: (1) The primary electroviscous effect arises in the inner part of the electrical double layer where the electrical field due to the mineral surface charge polarizes the dipolar water molecules. It follows that water exhibits a higher viscosity in the vicinity of the mineral-water interface by comparison with that in the bulk pore water due to preferential orientation of the water molecules in this electrical field. (2)-The secondary electroviscous effect occurs in a porous medium where an electrical field of electrokinetic nature pushes the excess of ions of the electrical diffuse layer in a direction opposite to the applied pore fluid pressure gradient and thus tends to resist to the relative fluid flow [e.g., *Pride and Morgan*, 1991]. This phenomenon leads to an apparent enhancement of the viscosity of the pore fluid (or, equivalently, to an apparent decrease of the permeability of the porous medium [e.g., *Bernabé*, 1998]).

As mentioned by *Pride and Morgan* [1991] this lexicon (used in colloidal chemistry) may be confusing since the secondary effect can be sometimes important for small pore radii (like those associated with the narrow grain-to-grain contacts discussed in section 2), whereas the primary effect is most of the time, unimportant and can be safely ignored. Clearly only the primary electroviscous effect is relevant to the discussion of the water viscosity and silica diffusivity inside the grain-to-grain contacts. However, the formula discussed by *Rutter* [1976, equation (12)] refers to the secondary electro-viscous effect. This important question concerning how the diffusivity of the solute is affected by various phenomena has never been seriously studied in previous works aimed to understand PPST. We describe in the sections 3.1-3.3 what are the factors that could influence silica diffusivity at the grain-to-grain contacts of a compacting quartz aggregate.

3.1. First ElectroViscous Effect

The influence of the electrical field of the electrical double layer upon the true viscosity of water in the vicinity of the mineral-water interface can be modeled using an expression provided by *Andrade and Dodd* [1951]

$$\eta_f(\chi) = \eta_f\left[1 + f\left(\frac{d\varphi(\chi)}{d\chi}\right)^2 + \ldots\right], \tag{32}$$

where η_f is the dynamic viscosity of the fluid in the absence of electric field, φ is here the electrical potential in the electrical double layer, χ is the local distance perpendicular to the mineral water interface (see Figure 2), and $f \approx 1 \times 10^{-17}$ m^2 V^{-2} [*Hunter*, 1966] is the electroviscous coefficient of water. The electrical potential distribution in the electrical double layer is given approximately by the Debye-Hückel equation [e.g., *Hunter*, 1966]

$$\varphi(\chi) \approx \varphi_0 \exp(-\chi / \chi_d), \tag{33}$$

where φ_0 is the electric potential at the mineral water interface and χ_d (in m) is the Debye screening length. The relationship between the dynamic viscosity of water and the solute diffusivity is given by the Nernst-Einstein relationship $D = (k_b T)/(6\pi \eta_f r)$ (where r is the hydrodynamic radius of the solute). From (32) and (33), the diffusivity of the solute in the vicinity of the surface is given by

$$D(0) \approx D_f\left(1 - f\left(\frac{\varphi_0}{\chi_d}\right)^2 + \ldots\right), \tag{34}$$

where D_f is the diffusivity of the solute in absence of electroviscous effect. The potential φ_0 and the length χ_d depend both on the salinity C_f according to $\varphi_0 = b \log_{10} C_f + c$ and on $\chi_d^{-1} = d\,(C_f)^{-1/2}$ according to (14) and (15), respectively (b, c, and d correspond to various constant parameters). Therefore at low salinity the potential φ_0 is high but χ_d^{-1} is very small and the electroviscous effect is small. At high salinity, φ_0 is very low, but χ_d^{-1} is high and according to (34) the electroviscous effect is small. The electroviscous effect reaches a maximum value for an intermediate salinity given by $C_f = 10^{-(c/b + 2/e)}$ with e = 2.303. This salinity is equal to 6.7 x 10^{-2} mol L^{-1} and at this salinity the relative variation of the diffusivity $(D(0) - D_f)/D_f$ is smaller than 1%. Therefore we conclude that the electroviscous effect is a very small effect even inside the inner part of the electrical double layer. The influence of the temperature would not change this fact because the influence of the temperature upon potential φ_0 and χ_d is rather small. Consequently, the electroviscous explanation cannot be used to justify a decrease of the diffusivity by 5 orders of magnitude. Mention should be made that actually water behaves quite normally right down to the last layers in contact with a silica surface [e.g., *He et al.*, 1987].

3.2. Second ElectroViscous Effect

The second electroviscous effect is actually an electrokinetic phenomenon [e.g., *Pride and Morgan*, 1991; *Bernabé*, 1998]. In a porous medium the hydraulic and electric charge flows are coupled due to the presence of the electrical double layer. Such coupling can be written by two coupled constitutive relationships for the electrical current density $\mathbf{j}$ (in A m^{-2}) and the water flux (Darcy velocity) $\mathbf{u}$ (in m s^{-1}) [e.g., *Revil et al.*, 1999b]

$$\mathbf{j} = -\sigma\nabla\psi - \ell\nabla p, \tag{35}$$

$$\mathbf{u} = -\ell \nabla \psi - \frac{k}{\eta_f} \nabla p, \tag{36}$$

where σ is the effective electrical conductivity of the porous medium (in S m^{-1}), k is its permeability (in m^2), ℓ is the electrokinetic coupling coefficient (in m^2 V^{-1} s^{-1}) between the electrical current density and the water flux, and ψ (in V) and p (in Pa) are the electrical potential and fluid pressure in the system [e.g., *Revil et al.*, 1999b]. In the absence of electrical current density (j = 0) the water flux equation can be rewritten as the classical Darcy's law

$$\mathbf{u} = -\frac{k}{\eta} \nabla p, \tag{37}$$

where η is an apparent pore fluid viscosity related to the true pore fluid viscosity η_f by

$$\eta = \eta_f (1 - \mathrm{R})^{-1}, \tag{38}$$

$$\mathrm{R} \equiv \frac{\ell^2 \eta_f}{k \sigma}. \tag{39}$$

We apply now (38) and (39) to the case of a grain-to-grain contact to compute the apparent viscosity of the fluid in such a contact (Figure 7). For such a case the equations given by *Revil et al.* [1999b] can be modified to obtain an appropriate form for the parameters k, σ, and ℓ at a grain-to-grain contact:

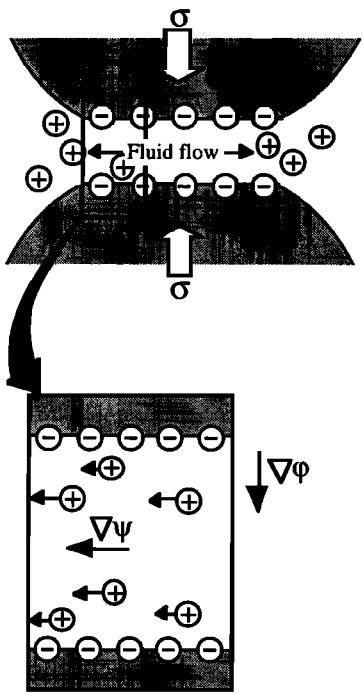

Figure 7. Sketch of the electrokinetic effect at a stressed grain-to-grain contact. The fluid flow induced by the compression of the gel layer present at a stressed grain-to-grain contact is responsible for an electrokinetic effect, which reduces the apparent viscosity of the gel layer. The electrical fields - $\nabla\varphi$ and -$\nabla\psi$ are the electrical field associated with the electrical double layer and the electrical field associated with the electrokinetic coupling, respectively. These two electrical fields are perpendicular to each other. The total electrical potential inside the electrical double layer is the sum of the electrical potentials φ and ψ.

$$k = \omega^2 / (12\, \alpha_S^2), \tag{40}$$

$$\sigma = \left(\sigma_f + 2\Sigma_S / \omega\right) / \alpha_S^2, \tag{41}$$

$$\ell = \varepsilon_f \varphi_0 / (\eta_f \alpha_S^2), \tag{42}$$

where σ_f is the electrical conductivity of the brine (in S m^{-1}) and α_S (≥ 1) is the (dimensionless) tortuosity of the flow/diffusive pathways inside the grain-to-grain contact, which replaces here the concept of electrical formation factor in porous media [e.g., *Revil et al.*, 1999b]. The tortuosity accounts for the increase in grain boundary diffusion path length over that given by a straight-line path along the grain boundary. The term Σ_S (in S) in (41) is the specific surface conductivity, which represents surface electrical conductivity associated with counterion migration in the Stern layer [e.g., *Revil and Glover*, 1998; *Revil et al.*, 1999a]. Note that surface conductivity was neglected in the equation used by *Rutter* [1976, equation (12)]. However, *Revil et al.* [1999a, Figure 5] have shown that, at 25°C and for silica, Σ_S is in the range (3-9) x 10^{-9} S and Σ_S increases with the temperature. This surface conductivity is equivalent to a bulk conductivity ($2\,\Sigma_S / \omega$) inside the grain-to-grain contact equal to several siemens per meter, which is far from being negligible by comparison with σ_f which is often much smaller than 1 S m^{-1}. Using (38)-(42), we obtain

$$\eta = \eta_f \left(1 - \frac{12\, \varepsilon_f^2 \varphi_0^2}{\eta_f \omega^2 \left(\sigma_f + 2\Sigma_S / \omega\right)} \right)^{-1}, \tag{43}$$

Once linearized, (43) leads to

$$\eta = \eta_f + \mathrm{R}', \tag{44}$$

$$\mathrm{R}' \equiv \eta_f \mathrm{R} = \frac{12\, \varepsilon_f^2 \varphi_0^2}{\omega^2 \left(\sigma_f + 2\Sigma_S / \omega\right)}, \tag{45}$$

which is basically the formula used by *Rutter* [1976, equation (12)] to argue that the diffusivity of silica at the grain-to-grain contacts is 5 orders of magnitude smaller than in the bulk water (except that surface conductivity was neglected in the expression that he used). The potential φ_0 increases as the salinity decreases, and this is the opposite for both the brine and surface conductivities. Therefore according to (45) the second electroviscous effect is maximum at low salinities. Taking the following set of parameters which are believed to be representative of the grain-to-grain contacts at low salinity ~10^{-5} mol L^{-1} (φ_0 = -120 mV, Σ_S = 3 x 10^{-9} S, ω = 2 nm, σ_f = 10^{-4} S m^{-1}, η_f = 0.9 x 10^{-3} Pa s at 25°C), we obtain R' = 7x10^{-3} Pa s, which represents an increase of ~1 order of magnitude of the apparent viscosity. At high salinity, e.g. 10^{-1} mol L^{-1} (φ_0 = -20 mV, Σ_S = 9 x 10^{-9} S, ω = 2 nm, σ_f = 1 S m^{-1}, η_f = 0.9 x 10^{-3} Pa s at 25°C), we obtain R' = 6 x 10^{-5} Pa s, which value is very small by comparison with η_f and therefore the second electroviscous effect can be neglected. We can already note that there are not 5 orders of magnitude of difference between the true and the apparent viscosity of the fluid inside the grain-to-grain contacts.

They are actually three mistakes made by Rutter in his argumentation. (1) The first point is related to the fact that (43) cannot be linearized when ω is small and the equation used by Rutter is valid only for a small viscosity increment. (2) The second mistake lies in the fact that surface conductivity was

neglected in the formula used by Rutter. As shown previously for narrow pores, surface conductivity represents a more important contribution to the total effective conductivity of the grain-to-grain contact than the brine conductivity. (3) The third point is related to the fact that the apparent viscosity appearing in the analysis of the second electroviscous effect is only a mathematical trick in order to rewrite the Darcy equation in a more familiar form. The true fluid viscosity is not affected by this phenomenon (and therefore the true diffusivity of the solute is not affected by the second electroviscous effect). Indeed, contrary to the primary electroviscous effect, which affects the true water viscosity, the second electroviscous effect leads only to an apparent enhancement of the viscosity of water in terms of flow rate.

Therefore the second electroviscous effect would have no influence upon the true diffusivity of silica at the grain-to-grain contacts.

3.3. Diffusivity of Silica at the Grain Contacts

We showed in sections 3.1 and 3.2 that silica diffusivity inside the grain-to-grain contacts is not affected seriously by the so-called electroviscous effect. This does not mean that other phenomena do not play any role upon this parameter. For example, the effective diffusivity of the solute at the grain-to-grain contacts is directly affected by the tortuosity of the diffusion pathways. The solute diffusivity D at the grain-to-grain contacts is related to the diffusivity of the solute in the bulk water D_f by [e.g., *Mullis*, 1991]

$$D = D_f / \alpha_S^2, \tag{46}$$

where $\alpha_S \geq 1$ is the tortuosity of the diffusion pathways along the grain-to-grain contacts. The tortuosity of the diffusion pathways at the grain-to-grain contacts results from the tortuosity associated with the presence of the polysilicic hairs and that associated with the roughness of the grain-to-grains contacts themselves. *Brady* [1983] has shown for a set of simplified, but plausible, grain shapes and aggregate geometries that ($1/\alpha_S^2$) lies in the range 0.9-0.3.

In addition to the tortuosity the diffusivity at the grain-to-grain contacts is affected by the ionic strength in these contacts, which is different from the ionic strength in the bulk pore water outside the grain-to-grain contacts. Indeed, there is generally an increase of the salinity (ionic strength) in the electrical diffuse layer. The total ionic concentration at the grain-to-grain contacts is such that the total charge in the electrical diffuse layer is equal in magnitude (and opposite in sign) to the surface charge at the mineral-water interface to insure electroneutrality. A mean salinity (in mol L^{-1}) inside the grain-to-grain contacts is roughly given by

$$\overline{C}_f = \frac{2 Q_S}{10^3 N e \omega}, \tag{47}$$

where the factor 2 is coming from the fact that there are two surfaces, 10^3 N e is a conversion factor, N is Avogadro's number (6.02 x 10^{23} mol^{-1}), and Q_S (in C m^{-3}) is the charge density of counterions inside the diffuse part of the electrical double layer [e.g., *Revil et al.*, 1999b]. This charge density can be evaluated by titration experiments such as reported by *Michael and Williams* [1984] and shown in Figure 8. Taking ω = 2 nm and Q_S = 5 x 10^{-2} C m^{-2} and 25 x 10^{-2} C m^{-2}, we found an equivalent salinity equal to 0.5 and 2.6 mol L^{-1}, respectively. The influence of this salinity upon the true viscosity of the fluid at the grain-to-grain contacts can be evaluated by finding a relationship between the salinity of an electrolyte and its dynamic viscosity. Experimental data concerning the influence of the salinity upon the viscosity of a NaCl brine solution can be represented accurately by (valid for salinity up to 6 mol L^{-1})

$$\eta_f(\overline{C}_f) = \eta_f\left(1 + \gamma_1 \overline{C}_f + \gamma_2 \overline{C}_f^{\,2} + ...\right), \tag{48}$$

where η_f is the viscosity of distilled water, $\gamma_1 \approx 0.034$ (mol L^{-1})$^{-1}$, and $\gamma_2 \approx 0.029$ (mol L^{-1})$^{-2}$. Using this formula and the equivalent salinity determined above at the grain-to-grain contacts, it results that the relative viscosity increase of the fluid inside the grain-to-grain contact is ~30%. This would reduce the diffusivity of the solute at the grain-to-grain contacts by the same ratio.

Therefore, according to the previous analysis the combined effect of the tortuosity and ionic strength at the grain-to-grain contacts reduces the diffusivity of the solute by roughly 1 order of magnitude, not more. However how does such a value compare with direct laboratory experiments of ion diffusivity at the grain-to-grain contacts of quartz aggregates? Note that only the product (ω D) can be determined experimentally through pressure solution experiments and therefore a value of ω has to be assumed (taken usually in the range 1-3 nm) to determine ion diffusivity inside the grain-to-grain contacts. Using the results reported by *Rutter* [1976] and *Gratier and Guiguet* [1986], *Renard et al.* [1997] found $D = 10^{-(10 \pm 1)}$ m^2 s^{-1}, which corresponds roughly to a silica diffusivity 1 order of magnitude smaller than the diffusivity of silica in the bulk pore water. This is in perfect aggrement with the present study. At

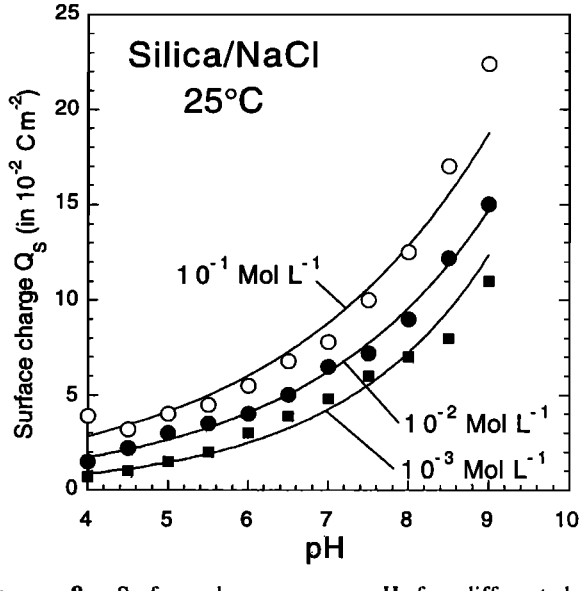

Figure 8. Surface charge versus pH for different brine salinity. At low pH values, the silica surface is flat and the density of silanol surface site is relatively low. At high pH values, the surface of silica become hairy due to the presence of a brush layer of poly-silicic polymers forming a gel layer of hydrolyzed material due to dissolution of the surface. This gel layer is responsible for a high charge density at the surface of silica. The experimental data are from *Michael and Williams* [1984].

the opposite, *Farver and Yung* [1991] provided grain boundary oxygen diffusivity data in fine grained quartz novaculite aggregates, which are ~6 orders of magnitudes less than ionic diffusion coefficients in the free pore water in the temperature range 450-800°C. According to S. Zhang (personal communication, 2000), silica metasomatism experiments show that silica diffusivity is ~4 orders of magnitude less than in the free pore water at 700°C. These values are much lower than reached in the present study. However, a comparison between these results and the present work would require, for example, to know if the gel layer film discussed in section 2 is stable at high temperatures (> 400°C) and pressures. Such information is still unavailable at our state of knowledge. However, we have shown in this section that the electroviscous explanation advanced by Rutter to justify small silica diffusivity at grain-to-grain contacts can be safely ruled out. It is also clear that the present scenario should be tested further before to reach any definite conclusions about the value of silica diffusivity at the grain-to-grain contacts during deformation of a quartz aggregate by PPST. However, we will see in section 5 that a relatively normal value for the silica diffusivity is consistent with laboratory experiments of quartz deformation by PPST.

4. Constitutive Relationship

This section is dedicated to the determination of a new constitutive equation describing the bulk compaction of a quartz aggregate by PPST. Such an equation represents a relationship between the state variables (e.g., porosity and/or contiguity) of the system and its environment (e.g., stress and stress rate). Two types of constitutive equations have been used in the past to describe deformation of porous quartz aggregates by pressure solution. In a first set of papers a Newtonian constitutive law was used to interpret laboratory measurements [e.g., *Rutter*, 1976 and *Mullis*, 1991]. Later, *Palciauskas and Domenico* [1989] and *Stephenson et al.* [1992] used a purely plastic constitutive equation to describe sandstone equilibrium compaction over geologic timescales.

A Newtonian viscous law can fit most of the laboratory measurements reported in the literature. However it is not certain that such a viscous law would apply over geological timescales. It should be remembered that only short timescales are investigated through laboratory measurements even if the temperature is raised and accounting for the fact that PPST is partly a temperature activated phenomenon. Indeed, the temperature cannot be increased over 400°C because some other deformation processes start to become active at that temperature in a quartz sand [*Rutter*, 1976]. The point is that PPST would be nonviscous over long timescales. However what does a long timescale means? *Revil* [1999] derived a characteristic timescale τ at which pressure solution starts to be nonviscous. This characteristic timescale depends strongly upon the temperature and the grain size. Most of the experiments reported in the literature correspond to timescales of observation much smaller than τ. Therefore it is not surprising to see that, so far, pressure solution has been mainly described as a viscous phenomenon by research scientists performing laboratory experiments. A research work looking at sandstone compaction in conditions such as the duration of the experiment is greater than τ has still to be carried out. Such an experimental work would require to use fine grain quartz aggregates to reduce the characteristic timescale τ and relatively high temperature (say ~300°C)

Palciauskas and Domenico [1989] and later *Stephenson et al.* [1992] were the first to contest the use of a viscous law as the correct rheology describing PPST over geological timescales. Instead, they used a purely plastic law to interpret sandstone bulk deformation by PPST in sedimentary basins. Looking at compaction trends for clean sandstones in different sedimentary basins characterized by the same geothermal gradient G (Figure 9), we observe that the compaction trend does not depend seriously on the age of the formations as it should be in the case for a viscous rheological behavior such as used by *Angevine and Turcotte* [1983]. A similar conclusion about the fact that the hydrostatic porosity-depth trend of clean sandstones is relatively independent of the age of the formations was also reported by *Maxwell* [1964] and cited later by *Palciauskas and Domenico* [1989]. It is quite surprising that this observation is never cited by research scientists using the viscous law to describe compaction path of clean sandstones in sedimentary basins. Indeed, this observation contradicts directly the assumption that the viscous behavior observed during laboratory experiments applies over geological timescales. At the opposite, this observation supports the assumptions made by *Palciauskas and Domenico* [1989] and *Stephenson et al.* [1992].

In a preliminary work, *Revil* [1999] started to unify the two previous rheological behaviors into a new formulation of the

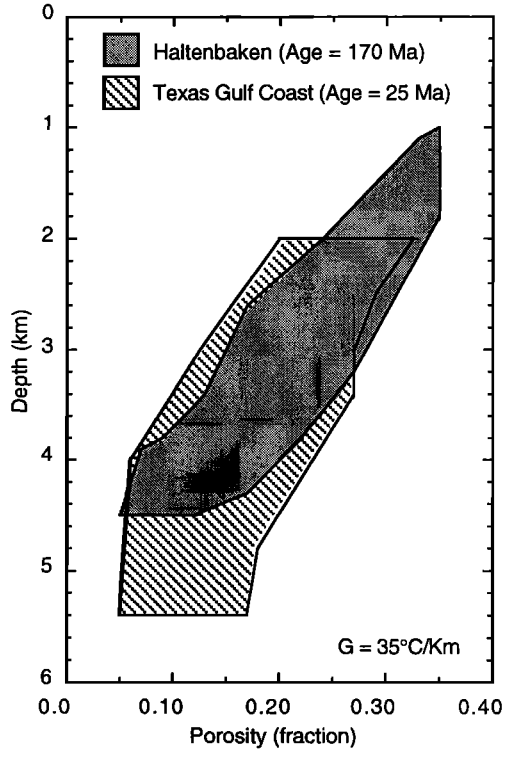

Figure 9. Porosity versus depth for clean sandstones for hydrostatic pore fluid pressure conditions. The compaction trend of the clean sandstone present in the Haltenbaken formation (~170 Ma) is compared with the compaction trend of the clean sandstone in the Texas Gulf Coast (~25 Ma). Both trends are very similar. Therefore the compaction trend for clean sandstones does not depend on the age of the formation. The assumption of a viscous behavior implies a very strong dependence of the compaction trend with time. At the opposite, plastic equilibrium leads to compaction trend independent of time.

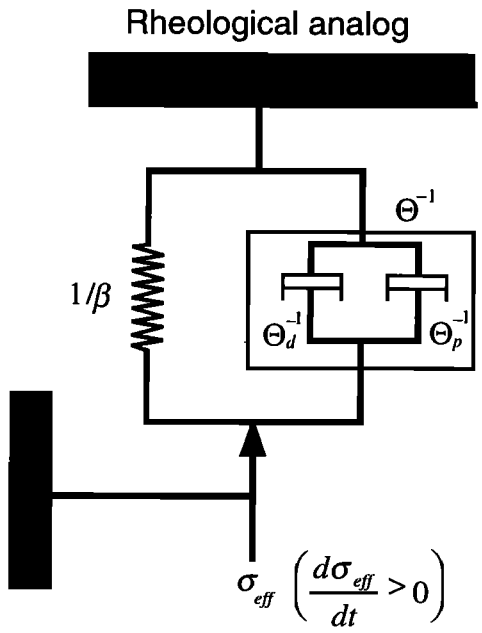

Figure 10. The deformation of a representative elementary volume of a quartz sand follows a poroviscoplastic (Voigt-type) rheological behavior. The spring models the plastic equilibrium state, whereas the dashpots represent the kinetics of PPST at the grain-to-grain contacts (the dashpots "p" and "d" correspond to dissolution/precipitation chemistry and diffusion limited processes, respectively).

rheology describing PPST. This was accomplished using a Voigt-type poroviscoplastic law (Figure 10). Let us recall how such a macroscopic constitutive equation can be formulated. The bulk compaction of a quartz aggregate by PPST under the influence of the hydrostatic part of the stress tensor corresponds to a one-dimensional flow law in which stress and strain are treated as scalar quantities. The constitutive equation is expected to be a scalar function of the state variables:

$$f(e,\dot{e},\sigma_{eff},\dot{\sigma}_{eff},T,S)=0, \tag{49}$$

where e and $\dot{e}$ are the strain and strain rate (defined properly below), T is the absolute temperature, and S is a structural parameter depending on the textural and chemical properties of the quartz aggregate. The constitutive equation (49) represents a surface in the six-dimensional parameter space of the state variables. All equilibrium states lie on this surface. During ductile flow the value of the state variables are constrained to remain on this surface. Therefore a small change in the following state variables yields the following relationship in isothermal conditions:

$$f_e de + f_{\dot{e}} d\dot{e} + f_{\sigma_{eff}} d\sigma_{eff} + f_{\dot{\sigma}_{eff}} d\dot{\sigma}_{eff} + f_S dS = 0, \tag{50}$$

$$f_x \equiv \partial f / \partial x. \tag{51}$$

This is the differential form of the constitutive equation. The partial derivative of this equation are functions of the state variables and they can be determined by various experiments in which small changes are made in some of the state variables. One of these useful experiments is the so-called creep experiment in which the effective stress follows (4) (see *Gangi* [1981] and *Ivins and Sammis* [1996]). In addition, we assume that pressure solution can be described by a first-order kinetics law. If the constitutive law is viscous in the first stage of deformation and plastic in the equilibrium state, a viscoplastic Voigt-type rheology would satisfy to these conditions. Assuming a time-independent structural parameter and with an isothermal condition, equation (50) yields (after dividing through by dt and integrating)

$$\frac{de}{dt} + \mathrm{Re}\ e = a\delta(t) + b\mathrm{H}(t), \tag{52}$$

$$\mathrm{Re} = f_e / f_e, \tag{53}$$

$$a = -\sigma_{eff}\left(f^0_{\dot{\sigma}_{eff}} / f^0_e\right), \tag{54}$$

$$b = -\sigma_{eff}\left(f^0_{\sigma_{eff}} / f^0_e\right), \tag{55}$$

$$f^0_x(t) \equiv \frac{\partial f}{\partial x}(0), \tag{56}$$

where $\delta(t)$ is the delta function, a and b are constant parameters, and Re is constant in the case where first-order kinetics is assumed to hold. Of course, Re can have much more complicated variations with respect to the state variables. We will show in a future paper that accounting for the texture of a porous aggregate undergoing compaction leads to a dependency of Re with another state variable, the grain-to-grain contiguity. The poroviscoplastic rheological model described in Figure 10 yields

$$\mathrm{Re} = 1/\tau, \tag{57}$$

$$a = 0,\ b = -\left(\frac{\phi_0}{1-\phi_0}\right)\sigma_{eff}\Theta, \tag{58}$$

where ϕ_0 is the porosity in the reference state defined in section 2 and $\tau = \Theta / \beta$ is the characteristic time constant of the rheological model shown in Figure 10. Therefore (52)-(58) yield

$$\tau\frac{de}{dt} + e = -\left(\frac{\phi_0}{1-\phi_0}\right)\beta\sigma_{eff}\mathrm{H}(t). \tag{59}$$

I define now the porosity strain $\tilde{\phi} > 0$ at time t:

$$\tilde{\phi}(t) \equiv [\phi_0 - \phi(t)] / \phi_0, \tag{60}$$

where $\phi(t)$ is the porosity at time t. I used the assumption of silica mass conservation inside a Lagrangian representative elementary volume of the compacting quartz aggregate. This closed system assumption is used to show that the solid mass redistribution due to pervasive pressure solution transfer is local; that is, conservation of silica mass in the representative elementary volume is assumed. This can be achieved if the pore water is always at saturation with respect with silica (at pore pressure and temperature) and if any additional material diffusing out of the grain-to-grain contacts is precipitated out quickly, before the fluid carrying it is expelled out of the representative elementary volume. Of course, the pore water itself can move in or out from the representative elementary volume (drained condition). The grain mass in the reference and stressed states are written respectively by

$$m^0_g = \rho^0_g(1-\phi_0)V_0, \tag{61}$$

$$m_g = \rho_g(1-\phi)V, \tag{62}$$

where ρ_g is the grain density. The porosity ϕ, total bulk volume V, and mass change between the stressed state and the reference state are

$$\delta\phi \equiv \phi - \phi_0, \tag{63}$$

$$\delta V \equiv V - V_0, \tag{64}$$

$$\delta m_g = m_g - m_g^0. \tag{65}$$

I consider ρ_g = 2650 kg m^{-3} for quartz, independent of fluid pressure and confining stress; that is, the grain density change corresponding to a given effective stress change can be neglected in regard to the finite deformation associated with pressure solution. Because the deformation is referred to a reference state in which no stress is applied, the trace of the inelastic deformation tensor is $\varepsilon \equiv \delta V / V_0$ (note that we are only interested here in the influence of the isotropic components of the stress tensor, not in the influence of the deviatoric components). In a Lagrangian framework associated with the deformation of the REV, the mass conservation of silica, expressed by $\delta m_g = 0$, yields

$$\frac{\varepsilon}{1+\varepsilon} \equiv \left(\frac{\delta V}{V}\right) = \frac{\phi - \phi_0}{1-\phi_0}. \tag{66}$$

Equation (66) reduces to $\varepsilon = dV/V = d\phi/(1-\phi)$ only for infinitesimal deformations. The finite strain and strain rate are given by

$$e(t) \equiv \frac{\delta V}{V} = -\frac{\phi_0 - \phi(t)}{1-\phi_0} = -\left(\frac{\phi_0}{1-\phi_0}\right)\tilde{\phi}(t), \tag{67}$$

$$\dot{e}(t) \equiv \frac{de}{dt} = -\left(\frac{\phi_0}{1-\phi_0}\right)\left(\frac{d\tilde{\phi}(t)}{dt}\right). \tag{68}$$

Substituing (67) and (68) into (59) yieds

$$\tau \frac{d\tilde{\phi}(t)}{dt} + \tilde{\phi}(t) = \beta \sigma_{eff} \mathrm{H}(t). \tag{69}$$

For the creep experiments the solution of this differential equation is given by

$$\tilde{\phi}(t) = \beta(t)\sigma_{eff}\mathrm{H}(t), \tag{70}$$

where $\beta(t)$ is the creep function (Figure 11) given by [*Revil*, 1999]

$$\beta(t) = \beta\left[1 - \exp(-t/\tau)\right], \tag{71}$$

$$\tau \equiv \beta / \Theta, \tag{72}$$

$$\beta = \frac{4\Omega}{\mathrm{E_m}(1 - T/T_\mathrm{m})}, \tag{73}$$

$$\Theta^{-1} = (\Theta_d)^{-1} + (\Theta_p)^{-1}, \tag{74}$$

$$\Theta_d = \left(\frac{32\,\Omega}{k_b\,T}\right)\frac{C_S^0\,\omega D}{\rho_g\,d^3}, \tag{75}$$

$$\Theta_p = \left(\frac{3\Omega^2 N}{k_b T}\right)\frac{k_+}{d}, \tag{76}$$

where β is the long-term poroplastic compressibility or compaction coefficient (as the term compressibility is generally reserved for poroelastic (reversible) deformation), $\mathrm{E_m}$ and T_m are the heat and temperature of fusion of SiO_2 respectively ($\mathrm{E_m}$ = 8.57 kJ mol^{-1}, T_m = 1883 K) and T (in K) is the temperature, k_b is the Boltzmann constant (1.381 x 10^{-23} J K^{-1}), Ω is the molecular volume of the solid phase (3.77 x 10^{-29} m^3), C_S^0 (in kg m^{-3}) is the solubility of the grain surface in the pore water solution in equilibrium with quartz at fluid pressure and temperature, and d is the average diameter of the grains in the porous aggregate. The parameter k_+ (in mol m^{-2} s^{-1}) is the dissolution rate constant of the chemical reaction of dissolution/precipitation of quartz:

$$SiO_2(s) + 2H_2O \Leftrightarrow H_4SiO_4(aq). \tag{77}$$

Equations (75) and (76) are determined by equating the rate of work done by the effective stress to the rate of energy dissipation due to dissolution/precipitation processes and transport of the solute by diffusion along the grain-to-grain contacts.

Actually, there is a strong analogy between pervasive pressure solution such as described previously and thermally activated chemical transformations. Thermally activated transformations proceed at a certain reaction rate when the system is maintained at constant pressure and temperature. The reaction rate dX/dt is defined as the time derivative of the volume fraction of transformed phase at time t, $X = V/V_0$, where $V(t)$ is the volume of the transformed phase at time t and V_0 the initial volume. The kinetics of the isothermal reaction is

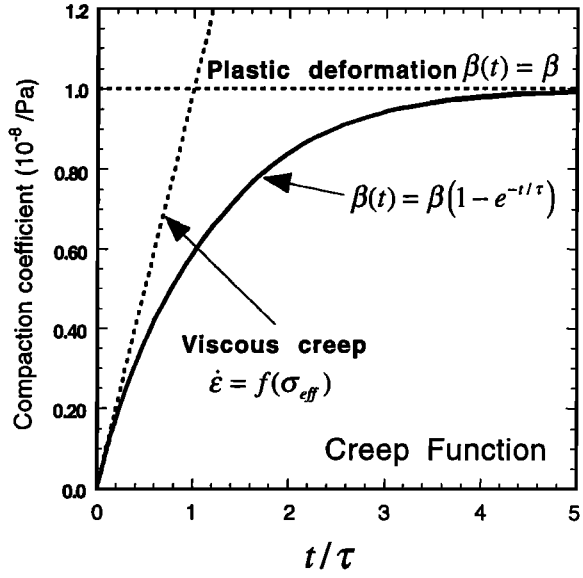

Figure 11. Creep function for pervasive pressure solution transfer for the rheology derived by *Revil* [1999]. For short timescales ($t/\tau << 1$) the inelastic deformation corresponds to viscous creep, and the relationship between the irreversible volumetric strain rate and the effective stress takes the form of a Newtonian linear viscous law. For long timescales ($t/\tau >> 1$) the deformation is purely plastic.

known when one knows $X(t)$. For first-order reaction the volume fraction as a function of time, $X(t)$, is a solution of a first-order linear differential equation written as

$$\frac{dX}{dt} = K(T)(1 - X(t)), \tag{78}$$

where $K(T)$ (in s^{-1}) is the reaction constant. Integration of this differential equation yields

$$X(t) = 1 - \exp(-t/\tau), \tag{79}$$

where $\tau = 1/K$ is the characteristic time for the reaction. This characteristic time gives an idea of the time-scale required to reach thermodynamic equilibrium. According to (79), pervasive pressure solution transfer of a quartz porous aggregate can be considered as a thermally activated deformation process, which proceeds at a certain deformation rate when the representative elementary volume is maintained at constant effective stress and temperature before to reach a thermodynamic equilibrium state. The characteristic time constant τ of the PPST problem corresponds to the timescale needed to reach compaction equilibrium.

We generalize now the previous approach for any effective stress history assuming that the effective stress history $\sigma_{eff}(t)$ is a positive function of time. The use of the Boltzmann superposition principle leads to a more general constitutive law between the porosity strain and the effective stress, which is given by [*Revil*, 1999]

$$\tilde{\phi}(t) = \beta(t) \otimes \frac{d\sigma_{eff}(t)}{dt} + \sigma_{eff}(t) \otimes \frac{d\beta(t)}{dt}, \tag{80}$$

where $\otimes$ is the finite convolution product and $\beta(t)$ is the creep function defined above. The finite convolution of two functions f and g is defined by

$$(f \otimes g)(t) = \int_0^t f(t')g(t-t')dt' . \tag{81}$$

Note that the multiplicative constants in (75) and (76) depend in principle on the texture of the porous aggregate, and especially on the grain-to-grain contiguity and the mean coordination number between the grains, which have not been included in the simple model presented here. A more complete model capturing the influence of the microstructure will be provided in a future paper in a way similar to that used recently by *Or* [1996] and *Guezzehei and Or* [2000], who studied the dynamics of soil coalescence governed by capillary and rheological processes.

Now I discuss the limiting step in the kinetics of PPST. In the models of *Weyl* [1959] and *Rutter* [1976], diffusion of the solute is assumed to take place through an adsorbed water film at the grain-to-grain contacts. It was also supposed that diffusion of the solute in this film is much slower than in the bulk water. Hence it has been widely accepted in the past that pressure solution transfer is a diffusion-limited process [e.g., *Rutter*, 1976]. This is in contradiction with more recent experimental studies [e.g., *Dewers and Hajash*, 1995]. In section 3, solute diffusion at the grain-to-grain contacts is shown to be relatively similar to that in the bulk pore water. It follows that pressure solution is not necessarily limited by the diffusion step and the dissolution/precipitation rate can control PPST in sedimentary basins [e.g., *Dewers and Hajash*, 1995; *Lander and Walderhaug*, 1999]. Below I discuss the conditions corresponding to diffusion or reaction-limited kinetics.

Using the dashpot analog of Figure 10, the effective viscosity η of the system is given by

$$\eta \equiv \frac{1}{\Theta} = \frac{1}{\Theta_d} + \frac{1}{\Theta_p}. \tag{82}$$

We can compare the order of magnitude of the two terms of (82) by defining the following nondimensional parameter

$$\gamma \equiv \frac{\Theta_d}{\Theta_p} \approx 11 \left(\frac{C_S^0 D_f \omega}{\rho_g d^2 \Omega k_+} \right). \tag{83}$$

The case $\gamma >> 1$ corresponds to reaction-limited kinetics for PPST, whereas the case $\gamma << 1$ corresponds to diffusion-limited kinetics. To evaluate γ, we need the temperature dependence of all the parameters involved in (83). As a first approximation, the parameters C_S^0, D, and k_+ involved in (83) have all an Arrhenius-type dependence with the temperature:

$$C_S^0(T) = C_0 \exp(-E_C/RT), \tag{84}$$

$$D_f(T) = D_0 \exp(-E_D/RT), \tag{85}$$

$$k_+(T) = k_+^0 \exp(-E_{k+}/RT), \tag{86}$$

where R is the universal gas constant (8.314 J $mol^{-1}K^{-1}$). For the solubility of quartz in distilled water, C_0 = 67.6 kg m^{-3} and E_C = 21.68 kJ mol^{-1} [*Iler*, 1979] and for the diffusivity of $Si(OH)_4$ $D_0 = 5.2 \times 10^{-8}$ m^2 s^{-1} and E_D = 13.5 kJ mol^{-1} (these values are determined from the values of the diffusivity of $Si(OH)_4$ in water corrected by the tortuosity at the grain-to-grain contacts equal to 2, see section 3). Note for comparison that *Dewers and Ortoleva* [1990, Appendix B] used $D_0 \sim 1 \times 10^{-8}$ m^2 s^{-1} and E_D = 40 kJ mol^{-1} and *Nakashima* [1995] used E_D = 15 kJ mol^{-1}. The data of *Dove and Crerar* [1990] for the surface kinetic coefficient k_+ of quartz in saline water lead to k_0^+ = 31.3 mol m^{-2} s^{-1} and E_{k+} = 71.3 kJ mol^{-1}. Equations (83)-(86) yield

$$\gamma = \gamma_0 \exp\left(\frac{E}{RT}\right), \tag{87}$$

$$\gamma_0 \equiv \frac{11\ C_0 D_0 \omega}{d^2 \rho_g \Omega k_+^0}, \tag{88}$$

$$E \equiv E_{k+} - E_C - E_D. \tag{89}$$

From equations (87)-(89) the domains corresponding to diffusion-limited and reaction-limited processes can be drawn as a function of the mean grain diameter, temperature, and grain-to-grain contiguity (Figure 12). At a given grain size, the increase of the temperature leads generally to a diffusion-limited process rather than a reaction-limited process for pressure solution in agreement with the concluding statements made by *Gratier and Gamond* [1990]. However, reaction-limited kinetics can be especially important in some conditions as some ions (like alumina and ferric ions) can slow down the kinetics of precipitation of the solute. This problem will be considered in more details in a future paper.

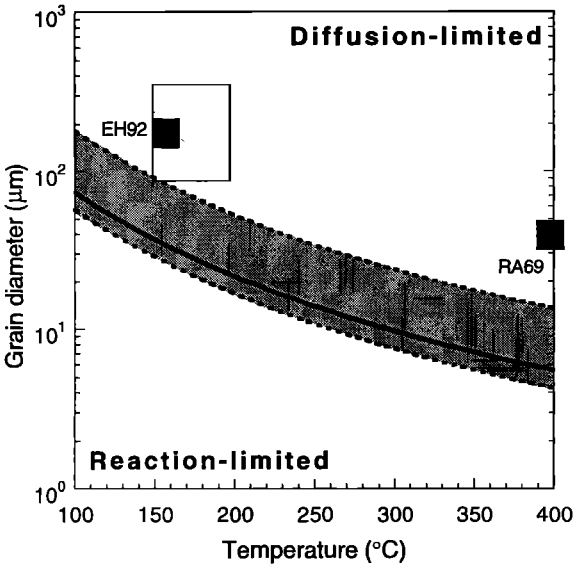

Figure 12. Kinetics of pressure solution. Pressure solution kinetics is limited by diffusion of the solute at the grain-to-grain contacts or by dissolution/precipitation of the grain-to-grain contact or by a composition of these two processes. This depends mainly on the mean grain diameter, and temperature, which increases during densification of a porous aggregate during deformation by pressure solution. The shaded square shown on the graph corresponds to the experimental data range (in terms of temperature and grain diameter) investigated by *Dewers and Hajash* [1995]. According to our model, both diffusion and reaction kinetics are important in the description of their results in agreement with the fact that they observed that the strain rate varies with the inverse of the grain diameter raised to the power 2.3, a value intermediate between 1 (reaction-limited) and 3 (diffusion-limited). The two solid squares represent the experimental conditions used by *Renton et al.* [1969] (labeled RA69) and *Elias and Hajash* [1992] (labeled EH92). Calculations are made with $\omega = 2$ nm and $\alpha_S = 2$.

5. Comparison With Experimental Data

Laboratory experiments and natural compaction in sedimentary basins occur in very different timescales. In sedimentary basins the burial compaction is a very slow process, and grains have time to adjust to the confining stress. *Stephenson et al.* [1992] have shown that the agreement between a plastic formulation and field data (from geographically diverse sandstone reservoirs ranging in age from Jurassic to Pleistocene) suggests that compaction equilibrium is reached in times that are short on the geological timescale. Therefore age is not the main factor in the chemical compaction of sandstones by PPST. The main conclusion reached by *Palciauskas and Domenico* [1989] and *Stephenson et al.* [1992] is that a plastic grain interpenetration model represents very well the long-term expression of pressure solution at compaction equilibrium in sedimentary basins over geological timescales.

Let us come back now to experimental works and specially to isothermal creep experiments. An isothermal creep experiment is one in which the stress on the rock sample is raised rapidly to some value and held there; that is, the effective stress history is given by (4). In this section we are going to compare our model and some creep experiments from the literature. As shown by equations (72)-(82) the characteristic time constant τ depends strongly on the temperature and the grain diameter. This is an advantage when we want to observe PPST at a reasonable time scales of few weeks or few months in the laboratory. However, because the activation energy entering in the viscosity is relatively small (< 80 kJ mol^{-1}), large temperature increments are required to produce a given deformation rate advantage. However temperature should not be too high because intracrystalline deformation processes can mask those associated with PPST. In addition, in experimental works the full load is sometimes applied at once, and the grains have no time to adjust themselves. It results in microfracturing at the grain contacts and/or grain crushing (cataclasis). This means that part of the work done by the effective stress is dissipated in this process. Keeping all these limitations in mind, in this section I compare the previous theoretical model with some experimental data from the literature in which experimental conditions (temperature, grain diameter, and time of observation) correspond to the limits $t(\text{obs}) \ll \tau$, $t(\text{obs}) \approx \tau$, and $t(\text{obs}) \gg \tau$, respectively, where $t(\text{obs})$ is the duration of the experiment (see Table 3). According to our model the porosity reduction of a porous aggregate submitted to an effective stress history given by (4) is analyzed in Figure 13. For short timescales by comparison with the relaxation time τ, the porosity decreases linearly with time, which is typical of a viscous deformation process. At timescales similar to τ, the porosity versus time trend is a decreasing exponential. For long timescales by comparison with τ, the porosity collapses nearly instantaneously (or at least very quickly) and then remains constant with time. In sections 5.1, 5.2, and 5.3 we show that laboratory experiments described in the literature are in agreement with the prediction of the model proposed in section 4.

5.1. Deformation at Short Timescales

Elias and Hajash [1992] have investigated the effect of compaction of a natural sandstone (grain size ~180-250 μm) at

Table 3. Computed Parameters for the Three Experiments Discussed in the Main Text

Parameter	EH[a]	RA[b]	LE[c]
d, μm	180	40	20
T, °C	150	400	700
σ_{eff}, MPa	69.9	41.4	170
Electrolyte	distilled water	0 5 M Na_2CO_3	distilled water
t(obs), days	198	40	~8
ϕ_0	0.33	0.54	0.41
ω, nm	4	2	4
D	D_f	D_f / 4	D_f
Θ_d^{-1}, Pa s	2.94 x 10^{16}	10.0 x 10^{13}	3.25 x 10^{11}
Θ_p^{-1}, Pa s	8.35 x 10^{15}	1.58 x 10^{12}	2.25 x 10^{10}
Θ^{-1}, Pa s	3.78 x 10^{16}	10.2 x 10^{13}	3.47 x 10^{11}
β, Pa^{-1}	1.37 x 10^{-8}	1.65 x 10^{-8}	2.19 x 10^{-8}
τ,	23 years	19.5 days	2 hours
$t(\text{obs})/\tau$	<< 1	~1	>> 1

[a] *Elias and Hajash* [1992].
[b] *Renton et al.* [1969].
[c] *Lockner and Evans* [1995].

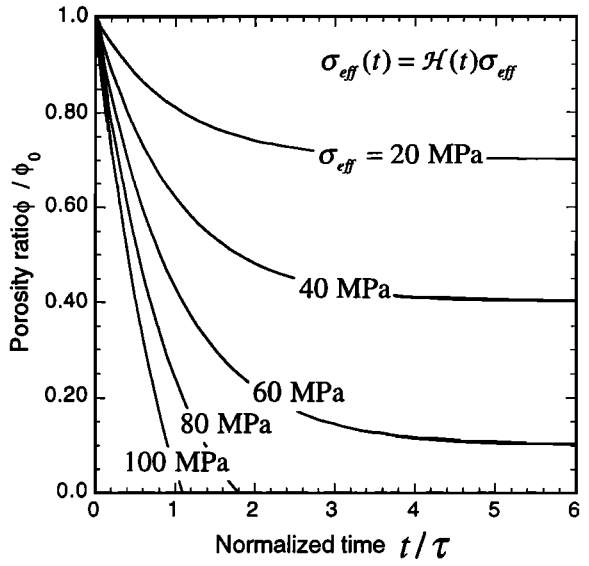

Figure 13. Normalized porosity versus normalized time for various values of the effective stress. The porosity decreases in an exponential way with time. For short timescales (by comparison with τ) the porosity changes linearly with time, whereas for long timescales the porosity decreases to a constant value ϕ_∞.

150°C over 5000 hours (t(obs) = 208 days) (see Figure 14). For such parameters and taking an average grain diameter of 250 μm, equation (73) yields a compaction coefficient β = 1.37 x 10^{-8} Pa^{-1} and a characteristic time constant of 23 years (see Table 3). This indicates clearly that t(obs) << τ. In this limit, equations (4), (70), and (71) lead to,

$$\phi = \phi_0\left(1 - \beta\sigma_{eff}\mathrm{H}(t)\frac{t}{\tau}\right). \qquad (90)$$

Consequently, the model predicts that for conditions corresponding to short time deformation by pressure solution with a constant effective stress, the porosity decreases linearly with time. This is in agreement with the experimental data of *Elias and Hajash* [1992]. From (90) the porosity decreasing rate is given by $d\phi/dt = -\phi_0\beta\sigma_{eff}/\tau = -\phi_0\Theta\sigma_{eff}$. The pore fluid pressure and the confining pressure used by *Elias and Hajash* [1992] are 34.96 MPa and 104.87 MPa, respectively, and consequently, the effective pressure is 69.9 MPa. The value of the viscosity $\eta = \Theta^{-1}$ and compaction coefficient β are determined in Table 3. The compaction rate is diffusion-limited; however, the kinetics of reaction cannot be neglected, as shown in Table 3. The uncompacted porosity deduced from Figure 14 is ϕ_0 = 0.328. From Figure 14 the data of *Elias and Hajash* [1992] lead to a porosity decreasing rate of -9.5 x 10^{-6} h^{-1}. Using an average grain diameter of 250 μm, the prediction leads $d\phi/dt$ = -2.2 x 10^{-6} h^{-1}, which is in relatively agreement with the experimental data.

5.2. Deformation at Intermediate Timescales

Renton et al. [1969] have studied the effect of texture and pore fluid composition on compaction for various types of sands. Porosity reduction of an angular quartz silt with an average grain diameter of 40 μm is reported in Figure 15. Their experiment is conducted at 400°C (not sufficient to induce intracrystalline plasticity) with 0.5 M Na_2CO_3 pore fluid solution at a hydrostatic pressure of approximately 41.4 MPa (see Figure 15). Using Table 3, this yields β = 1.65 x 10^{-8} Pa^{-1} and τ = 19.2 days. Consequently, because *Renton et al.* [1969] observed compaction during 40 days, their experimental conditions correspond to observation duration about the same magnitude as the time constant τ. Compaction was predominantly the result of pressure solution at the grain-to-grain contacts because no appreciable fracturing was observed and many concave-convex contacts and quartz overgrowths were observed between grains after the experiment. Assuming that the effective stress history is given by (4), (70), and (71) yield

$$\phi(t) = \phi_0\left[1 - \beta\left(1 - \exp\left(-\frac{t}{\tau}\right)\right)\sigma_{eff}\mathrm{H}(t)\right]. \qquad (91)$$

Therefore the porosity decreases exponentially with time. As shown in Figure 15, this is in good agreement with the experimental data shown by *Renton et al.* [1969]. A nonlinear fit of the data of *Renton et al.* [1969] (shown in Figure 15) using (91) leads to β = 1.89 x 10^{-8} Pa^{-1} and τ = 18.7 days in good agreement with the values β = 1.65 x 10^{-8} Pa^{-1} and τ = 19.5 days determined in Table 3 from the model derived in this paper. Consequently, the model is able to predict very well both the order of magnitude for the plastic compressibility and the characteristic time constant observed in Renton et al.'s experiment.

Material	d (μm)	T	σ_{eff}
Quartz sand	180-250	150 °C	69.9 MPa
Data from Elias and Hajash (1992)			

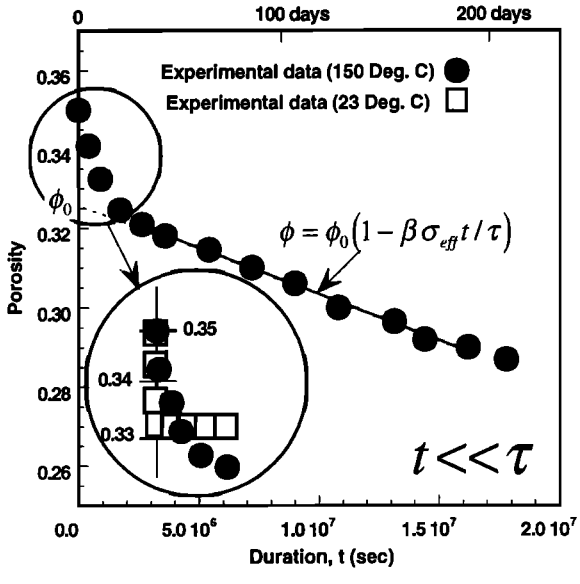

Figure 14. Comparison between the experimental data of *Elias and Hajash* [1992] and the prediction of the present model in the limit of small timescale of deformation (t(obs) << τ). Comparison with data at 25°C shows that the first stage of deformation corresponds to a small elastic contribution to deformation (pressure solution is inactive at 25°C at the timescale indicated). In the limit of small timescales of deformation t << τ and at a temperature of 150°C the experimental data show that the porosity varies linearly with the time of observation in agreement with the prediction of the model.

5.3. Deformation at Long Timescales

Lockner and Evans [1995] measured porosity reduction during the densification of ultrafine quartz powder (5-20 μm) saturated with distilled water at 700°C. At this temperature, pressure solution remains probably the main deformation mechanism even if other deformation processes are likely to be active [*Cox and Paterson*, 1991]. The experiment shown in Figure 16 corresponds to a densification of a quartz powder with an average grain diameter of 20 μm and an uncompacted porosity before densification of ϕ_0 = 0.41. The confining pressure is 200 MPa, the fluid pressure is 30 MPa, and therefore the effective differential stress is ~170 MPa. The duration of deformation is approximately t(obs) = 8 days. The conditions under which *Lockner and Evans* [1995] carried out their experiments are rather extreme in pressure, temperature, and grain diameter, and it is therefore very difficult to compare the present model with their experimental data other than qualitatively. Using the data listed in Table 3, we obtain β = 2.19 x 10^{-8} Pa^{-1} and τ = 2 hours. Consequently, the experiment of *Lockner and Evans* [1995] corresponds to the plastic limit t (≈ 8 days) >> τ ≈ 2 hours, and therefore the porosity is expected to decrease very quickly in the first hours of the experiment down to a constant value ϕ_∞ after 1 or 2 days. This is qualitatively in perfect agreement with the data reported by *Lockner and Evans* [1995, Figure 4].

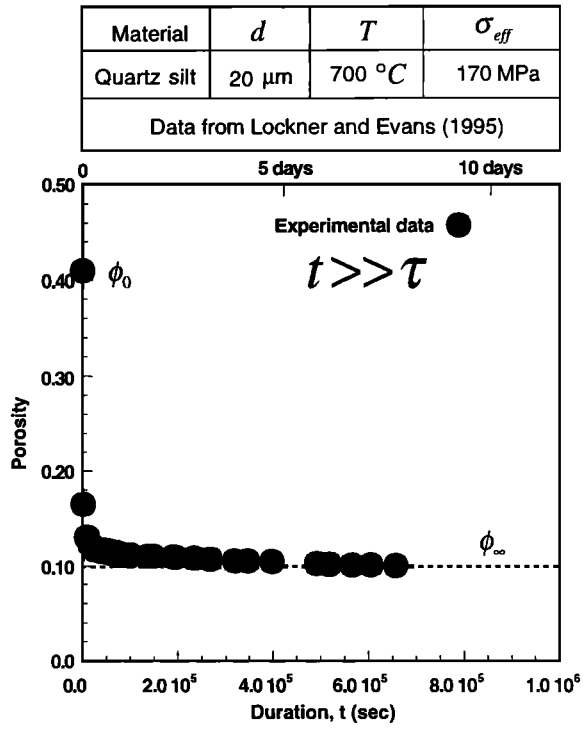

Figure 16. Comparison between the experimental data of *Lockner and Evans* [1995] and the prediction of the present model. In the limit where the characteristic relaxation time associated with pressure solution transfer is much smaller than the duration of the experiment (t(obs) >> τ), the model predicts that the porosity reaches quickly a constant value corresponding to the equilibrium limit of the model discussed in the main text.

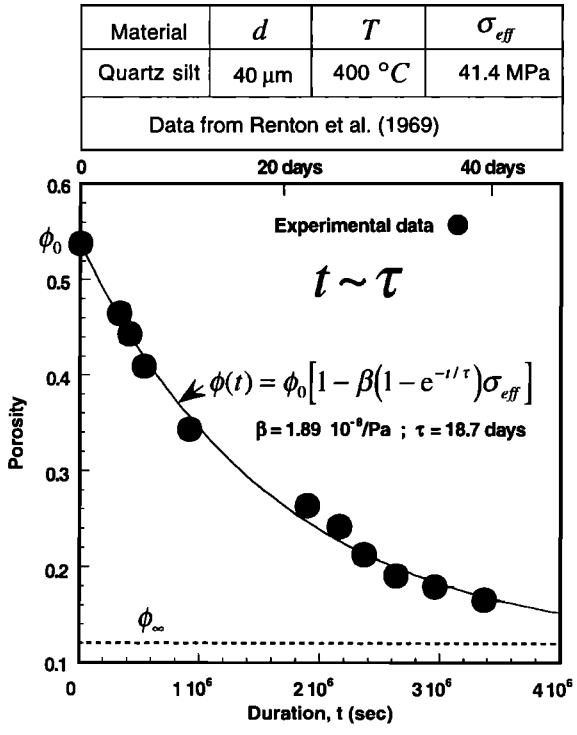

Figure 15. Comparison between the experimental data of *Renton et al.* [1969] and the prediction of the present model. In the limit where the characteristic relaxation time associated with pressure solution transfer has the same order of magnitude as the duration of the experiment (t(obs) ~ τ), the model predicts an exponential decrease of the porosity until equilibrium state is reached. This is in agreement with the data obtained by *Renton et al.* [1969]. Note that the timescale used cannot be compared directly with the timescale used in Figure 14 as the timescales of observation must be scaled by τ to be comparable at different temperatures.

6. Compaction Path in Sedimentary Basins

In this section we apply the model discussed in sections 4 and 5 to the compaction equilibrium path of a clean sandstone in a sedimentary basin undergoing positive sedimentation with time (i.e., no erosion is allowed). We assume that the compaction path can be described as a succession of equilibrium plastic states. In such a case the rhelogical model shown in Figure 10 reduces to the long-term plastic equilibrium limit given by

$$d\phi = -\phi_0 \beta \, d\sigma_{eff}, \tag{92}$$

where ϕ_0 is the porosity in a reference state (taken at the surface of the sedimentary basin at zero effective stress, β (in Pa^{-1}) is the compaction coefficient, and $\sigma_{eff} \approx \sigma - p$ (in Pa) is the differential effective stress. The differential effective stress is approximated by the difference between the lithostatic stress and pore fluid pressure. In hydrostatic pore fluid pressure conditions, it is straightforward to integrate (92) between the top surface of the sedimentary basin to depth z to obtain a porosity-depth relationship. In hydrostatic fluid pressure conditions the porosity, the fluid pressure, and the lithostatic pressure are given by

$$\phi_H(z) = 1-(1-\phi_0)\exp\left(\frac{z}{z_c}\right), \quad (93)$$

$$p_H = \rho_f g z, \quad (94)$$

$$P_H(z) = \int_0^z \rho g dz' = (\rho_g - \rho_f) g \int_0^z (1-\phi_H) dz', \quad (95)$$

$$P_H(z) = \rho_f g z + g(\rho_g - \rho_f)(1-\phi_0) z_c \left[\exp\left(\frac{z}{z_c}\right) - 1\right]. \quad (96)$$

respectively, where z is the depth (in m), g is the acceleration of gravity (9.81 m s^{-2}), ρ_g is the grain density (2650 kg m^{-3} for quartz), ρ_f is the density of the pore water, and z_c (in m) is a characteristic compaction lenght scale defined by

$$z_c = 1/\left[\phi_0(\rho_g - \rho_f) g \beta\right], \quad (97)$$

In Figure 17, I compare the hydrostatic porosity trend predicted by (93) to various sandstone compaction trends observed in sedimentary basins and reported in the literature. For each data set, a best fit of (93) is used to compute the porosity ϕ_0 and the compaction coefficient β. We found ϕ_0 in the range 0.39-0.45 and β in the range (1.6-2.6)x10^{-8} Pa^{-1}, which range is very similar to that determined in section 5 for laboratory data. The shape of the compaction curves is also very well reproduced by (93). Note that the shape of the compaction curve for clean sandstone is very different from that exhibited by shale along their compaction path. This has to do with the compaction phenomenon of interest: chemical compaction for clean sandstone and mechanical compaction for pure shale. We note that the sandstone compaction data shown in Figure 17 seems to exhibit a certain dependence of the compaction coefficient with the geothermal gradient. This dependence will have to be confirmed by further analysis.

We can extend equations (92)-(97) to the case of overpressured conditions resulting from compaction disequilibrium. In such a case, undercompaction and overpressuring result only from the inability of the sedimentary column to evacuate the pore fluid pressure in

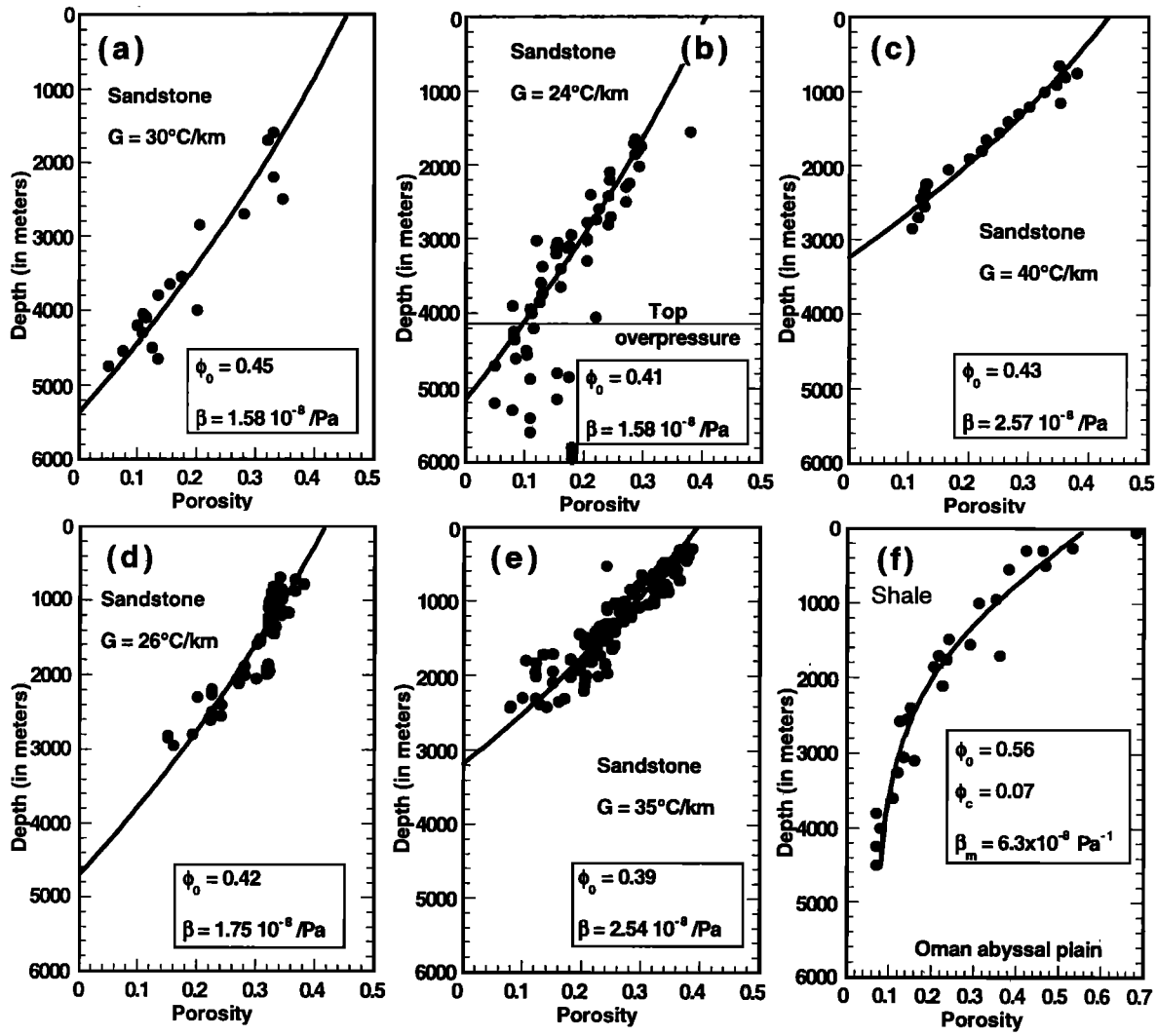

Figure 17. Compaction paths of clean sandstones in sedimentary basins. Data are from (a) *Robinson and Gluyas* [1982], (b) *Mudford and Best* [1989], (c) *Lerche* [1990], (d) and (e) *Magara* [1978], and (f) *Fowler et al.* [1985]. Note the difference between the shape of the compaction curves for sandstone and that for shale. The compaction curve for a shale corresponds to purely mechanical compaction (the curve in Figure 17f corresponds to a best fit using the mechanical compaction equation derived by *Revil* [2000]).

response to an increase of the sedimentary load due to sedimentation or tectonic stresses. The reasons for such an inability to dissipate the excess pressure lies in low-permeability sediments and/or capillary sealing. In such a case, the fluid and lithostatic pressures and the porosity are written, without loss of accuracy, by

$$p = p_H + \delta p, \tag{98}$$

$$P = P_H + \delta P, \tag{99}$$

$$\phi = \phi_H + \delta\phi, \tag{100}$$

where p_H is the hydrostatic fluid pressure, ϕ_H is the hydrostatic porosity, P_H is the lithostatic pressure in the hydrostatically pressured section, and the departures from the hydrostatic state are noted by $\delta\phi$ (excess porosity), δp (excess fluid pressure), and δP (excess lithostatic pressure). Using again the linear constitutive relationship between the effective stress and the porosity, the excess fluid pressure and the excess lithostatic pressure are related to the excess porosity by

$$\delta p(z) = \frac{1}{\phi_o \beta}\left(\delta\phi(z) - \frac{1}{z_c}\int_0^z \delta\phi(z')\,dz'\right), \tag{101}$$

$$\delta P = -\int_0^z \left(\rho_g - \rho_f\right) g\,\delta\phi\,dz'. \tag{102}$$

Equations (101) and (102) were already applied with sucess to downhole measurements previously by *Revil et al.* [1998, section 3 and Figure 10].

7. Concluding Statements

Pressure solution transfer at grain-to-grain contacts represents a compactional response of the porous aggregate in an attempt to increase the grain contact area (hence the contiguity) so as to redistribute the normal effective stress at the grain-to-grain contacts over a larger contact area. This process holds until a thermodynamic equilibrium state is reached. It was shown in this paper that (1) a thermodynamic compaction equilibrium is possible at the grain-to-grain contacts, which implies the use of a viscoplastic rheological model rather than the purely viscous or plastic models traditionally used, and (2) the diffusivity of the solute at the grain-to-grain contacts is relatively normal by comparison with that in water (and not 5 orders of magnitude smaller, as reported or cited in a number of previous papers). We have developed arguments for a Voigt-type viscoplastic rheological model to describe the bulk deformation associated with pervasive pressure solution transfer. This new model incorporates the two previous modeling attempts (viscous and plastic) within a unified approach. The proposed mechanism has roots in microprocesses occurring in the silica gel layer located at the grain-to-grain contacts. It is consistent with surface chemistry of silica and with the experimental results reported in the literature as well as with the compaction path followed by a clean (i.e., clay-free) sandstone in a sedimentary basin. Future extensions of this work will include (1) the use of a better textural model to appraise the influence of the grain-to-grain contiguity upon pressure solution transfer, (2) the inclusion of the effect of cataclasis upon the rheological behavior and porosity/stress change, which process is important to the understanding of fault gouge rheology [e.g., *Segall and Rice*, 1995, and *Kanagawa et al.*, 2000], (3) the influence of the deviatoric component of the effective stress tensor upon pervasive pressure solution, and (4) the influence of pore fluid chemistry (especially alumina and ferric ions) and clay coating-filling upon pervasive pressure solution transfer.

Acknowledgments. Olivier Brévart and Dominique Grauls are specially thanked for a grant from the compagny Elf Aquitaine during my stay at Cornell University in 1996-1997. This work is supported by the French National Research Council CNRS (Centre National de la Recherche Scientifique) in France and the GBRN (Global Basin Research Network) at Cornell University and the companies sponsoring the GBRN. Larry Cathles and Yves Bernabé are specially thanked for very fruitful discussions during various stages of this work. Jean-Pierre Gratier and Steven Hickman are thanked for a review of the first version of this paper. The second version of this paper benefited from critical reviews provided by Shuqing Zhang, Yasuko Takei, and the (anonymous) Associate Editor.

References

Abraham, T., S. Giasson, J. F. Gohy, and R. Jérôme, Direct measurements of interactions between hydrophobically anchored strongly charged polyelectrolyte brushes, *Langmuir, 16*, 4286-4292, 2000.

Andrade, E. N., and C. Dodd, The effect of an electric field on the viscosity of liquids. II, *Proc. Soc. London, Ser. A, 204*, 449-464, 1951.

Angevine, C. L., and D. L. Turcotte, Porosity reduction by pressure solution: A theoretical model for quartz arenites, *Geol. Soc. Am. Bull., 94*, 1129-1134, 1983.

Asaro, R. J., and W. A Tiller, Interface morphology development during stress corrosion cracking, part 1, via surface diffusion, *Metall. Trans., 3*, 1789-1796, 1972

Bear, J., and Y. Bachmat, *Introduction to Modelling of Transport Phenomena*, Kluwer Acad., Norwell, Mass., 1990.

Bernabé, Y., Streaming potential in heterogeneous networks, *J. Geophys. Res., 103*, 20,827-20,841, 1998.

Bos, B., C. J. Peach, and C. J. Spiers, Slip behavior of simulated gouge-bearing faults under conditions favoring pressure solutions, *J. Geophys. Res., 105*, 16,699-16,717, 2000.

Brady, J., Intergranular diffusion in metamorphic rocks, *Am. J. Sci., 283-A*, 181-200, 1983.

Colic, M., M. L. Fisher, and G. V. Franks, Influence of ion size on short-range repulsive forces between silica surfaces, *Langmuir, 14*, 6107-6112, 1998.

Cox, S. F., and M. S. Paterson, Experimental dissolution-precipitation creep in quartz aggregates at high temperatures, *Geophys. Res. Lett., 18*, 1401-1404, 1991.

De Boer, R. B., On the thermodynamics of pressure solution-Interactions between chemical and mechanical forces, *Geochim. Cosmochim. Acta, 41*, 249-256, 1977

Dewers, T , and A. Hajash, Rate laws for water assisted compaction and stress-induced water-rock interaction in sandstones, *J. Geophys. Res , 100*, 13,093-13,112, 1995.

Dewers, T., and P. Ortoleva, A coupled reaction/transport/mechanical model for intergranular pressure solution stylolites, and differential compaction and cementation in clean sandstones, *Geochim. Cosmochim. Acta, 54*, 1609-1625, 1990.

Dove, P. M., and D. A. Crerar, Kinetics of quartz dissolution in electrolyte solutions using a hydrothermal mixed flow reactor, *Geochim. Cosmochim Acta, 54*, 955-969, 1990.

Elias, B. P., and A. Hajash, Change in quartz solubility and porosity due to effective stress: an experimental investigation of pressure solution, *Geology, 20*, 451-454, 1992.

Ennis, J., L Sjöström, T. Åkesson, and B. Jönsson, Surface interactions in the presence of polyelectrolytes. A simple theory, *Langmuir, 16*, 7116-7125, 2000.

Farver, J. R., and R. A. Yund, Measurements of oxygen grain boundary diffusion in natural, fine grained, quartz aggregates, *Geochim. Cosmochim. Acta, 55*, 1597-1607, 1991.

Fowler, A. C., and X. Yang, Pressure solution and viscous compaction in sedimentary basins, *J. Geophys. Res., 104*, 12,989-12,997, 1999.

Fowler, S. R., R. S. White, and K. E. Louden, Sediment dewatering in the Makran accretionary prism, *Earth Planet. Sci. Lett., 75*, 427-438, 1985.

Gal, D., and A. Nur, Elastic strain energy as a control in the evolution of asymmetric pressure solution contacts, *Geology, 26*, 663-665, 1998.

Gangi, A. F., A constitutive equation for one-dimensional transient and steady state flow of solids, in *Mechanical Behavior of Crustal Rocks, The Handin Volume, Geophys. Monogr. Ser.*, vol. 24, edited by N. L. Carter, et al., pp. 275-285, Washington, D. C., 1981.

Gaudin, A. M., and D. W. Fuerstenau, Quartz flotation with anionic collectors, *Trans. Am. Inst. Min. Metall. Pet. Eng., 202*, 66-72, 1955.

Ghoussoub, J., Solid-fluid phase transformation within grain boundaries during compaction by pressuresolution , Ph.-D. thesis, 216 pp., Ecole Nat. des Ponts et Chaussées, Paris, France, 2000.

Gratier, J. P., Le fluage des roches par dissolution-cristallisation sous contrainte, dans la croûte supérieure (in French with English abstract), *Bull. Soc. Géol. Fr., 164*, 267-287, 1993.

Gratier, J. P., and J. F. Gamond, Transition between seismic and aseimic deformation in the upper crust, in *Deformation Mechanism, Rheology, and Tectonics*, edited by R. J. Knipe, and E. H. Rutter, *Geol. Soc Spec. Publ 54*, p. 461-474, 1990.

Gratier, J. P., and R. Guiguet, Experimental pressure solution-deposition on quartz grains: the crucial effect of the nature of the fluid, *J. Struct. Geol., 8(8)*, 845-856, 1986.

Guezzehei, T. A., and D. Or, Dynamics of soil aggregate coalescence governed by capillary and rheological processes, *Water Resour. Res., 36*, 367-379, 2000.

He, X. H., J. H. Cushman, and D. J. Diestler, Molecular dynamics of water near an uncharged silicate surface: Anisotropic diffusion, in *Flow and Transport Through Unsaturated Rocks, Geophys. Monogr. Ser.*, vol. 42, edited by D. D. Evans and T. J. Nicholson, pp. 61-71, AGU, Washington, D.C., 1987.

Heidug, W. K., Intergranular solid-fluid phase transformations under stress: the effect of surface forces, *J. Geophys. Res., 100*, 5931-5940, 1995.

Hickman, S. H., and B. Evans, Kinetics of pressure solution at halite-silica interfaces and intergranular clay films, *J. Geophys. Res., 100*, 13,113-13,132, 1995.

Horn, R. G., D. T. Smith, and W. Haller, Surface forces and viscosity of water measured between silica sheets, *Chem. Phys. Lett., 162*(45), 404-408, 1989.

Houseknecht, D. W., Intergranular pressure solution in four quartzose sandstones, *J. Sediment. Petrol., 58*, 228-246, 1988.

Hunter, R. J., The interpretation of electrokinetic potentials, *J. Colloid Interface Sci., 22*, 231-239, 1966.

Iler, R. K., *The Chemistry of Silica*, John Wiley, New York, 1979.

Israelachvili, J. N., *Intermolecular and Surface Forces*, 445 pp., Academic, San Diego, Calif., 1992.

Israelachvili, J. N., and H. Wennerstrom, Role of hydration and water structure in biological and colloidal interactions, *Nature, 379*, 219-225, 1996.

Ivins, E. R., and C. G. Sammis, Transient creep of a composite lower crust, 1, Constitutive theory, *J. Geophys. Res., 101*, 27,981-28,004, 1996.

Kanagawa, K., S. F. Cox, and S. Zhang, Effects of dissolution-precipitation processes on the strenght and mechanical behavior of quartz gouge at high-temperature hydrothermal conditions, *J. Geophys. Res., 105*, 11,115-11,126, 2000.

Kennedy, G. C., A portion of the system silica-water, *Econ. Geol., 45*, 629-653, 1950.

Lander, R. H., and O. Walderhaug, Predicting porosity through simulating sandstone compaction and quartz cementation, *AAPG Bull., 83*, 433-449, 1999.

Lehner, F. K., and J. Bataille, Non-equilibrium thermodynamics of pressure solution, *Pure Appl. Geophys., 122*, 53-85, 1984.

Lemée, C., and Y. Gueguen, Modeling of porosity loss during compaction and cementation of sandstones, *Geology, 24*, 875-878, 1996.

Lerche, I , *Basin Analysis, Quantitative Methods*, vol. 1, 562 pp., Academic, San Diego, Calif., 1990.

Li, H. C., and D. L. de Bruyn, Electrokinetic and adsorption studies on quartz, *Surf. Sci., 5*, 203-220, 1966.

Lockner, D., and B. Evans, Densification of quartz powder and reduction of conductivity at 700°C, *J. Geophys. Res., 100*, 13081-13092, 1995.

Magara, K., *Compaction and Fluid Migration, Practical Petroleum Geology*, 319 pp., Elsevier Sci., New York, 1978.

Maxwell, J. C., Influence of depth, temperature, and geologic age on porosity of quartzose sandstone, *AAPG Bull., 48*, 697-709, 1964.

Michael, H. L., and D. J. A. Williams, Electrochemical propoerties of quartz, *J. Electroanal. Chem.*, 179, 131-139, 1984.

Mudford, B. S., and M. E. Best, The Venture gas field, offshore Nova-Scotia: a case study of overpressuring in a region of low sedimentation rate, *AAPG Bull., 73*, 1383-1396, 1989.

Mullis, A. M., The role of silica precipitation kinetics in determining the rate of quartz pressue solution, *J. Geophys. Res., 96*, 10,007-10,013, 1991.

Nakashima, S., Diffusivity of ions in pore water as a quantitative basis for rock deformation rate estimates, *Tectonophysics, 245*, 185-203, 1995

Ninham, B W., and V. V. Yaminski, Ion binding and ion specificity: The Hofmeister effects and Onsager andLifshitz theories, *Langmuir, 13*, 2097-2108, 1997.

Or, D., Wetting-induced soil structural changes: The theory of liquid phase sintering, *Water Resour. Res., 32*, 3041-3049, 1996.

Palciauskas, V. V., and P. A. Domenico, Fluid pressures in deforming porous rocks, *Water Resour. Res., 25*, 203-213, 1989.

Parks, G. A., Surface and interfacial free energies of quartz, *J. Geophys. Res., 89*, 3997-4008, 1984.

Paunov, V. N., and B. P. Binks, Analytical expression for the electrostatic disjoining pressure taking into account the excluded volume of the hydrated ions between charged interfaces in electrolyte, *Langmuir, 15*, 2015-2021, 1999.

Pincus, P., Colloid stabilization with grafted polyelectrolytes, *Macromolecules, 24*, 2912-2919, 1991.

Pride, S., and F. D. Morgan, Electrokinetic dissipation induced by seismic waves, *Geophysics*, 56, 914-925, 1991.

Renard, F., P. Ortoleva, and J. P. Gratier, Pressure solution in sandstones: Influence of clays and dependence on temperature and stress, *Tectonophysics, 280*, 257-266, 1997.

Renton, J. J., M. T. Heald, and C. B. Cecil, Experimental investigation of pressure solution of quartz, *J. Sediment. Petrol., 39*, 1107-1117, 1969.

Revil, A., Thermal conductivity of unconsolidated sediments with geophysical applications, *J. Geophys. Res., 105*, 16,749-16,768, 2000.

Revil, A., Pervasive pressure-solution transfer: a poro-visco-plastic model, *Geophys. Res. Lett., 26*, 255-258, 1999.

Revil, A., and P. W. J. Glover, Nature of surface electrical conductivity in natural sands, sandstnes, and clays, *Geophys. Res. Lett., 25*, 691-694, 1998.

Revil, A., L. M. Cathles, S. Losh, and J. A. Nunn, Electrical conductivity in shaly sands with geophysical applications, *J. Geophys. Res., 103*, 23,925-23,936, 1998.

Revil, A., P. A. Pezard, and P. W. J. Glover, Streaming potential in porous media, 1, Theory of the zeta potential, *J. Geophys. Res., 104*, 20,021-20,031, 1999a.

Revil, A., H. Schwaeger, L M. Cathles, and P. D Manhardt, Streaming potential in porous media, 2, Theory and application to geothermal systems, *J. Geophys Res.. 104*, 20,033-20,048, 1999b.

Robinson, A., and J. Gluyas, Model calculations of loss of porosity in sandstones as a result of compaction and quartz cementation, *Mar. Pet. Geol., 9*, 319-323, 1992.

Rutter, E. H., The kinetics of rock deformation by pressure solution, *Philos. Trans., R. Soc. London, Ser. A, 283*, 203-219, 1976.

Rutter, E. H., Discussion on pressure solution, *J. Geol. Soc. London, 135*, 135, 1978.

Segall, P., and J. R. Rice, Dilatancy, compaction, and slip instability of a fluid-infiltrated fault, *J Geophys. Res., 100*, 22,155-22,171, 1995.

Skempton, A. W., Effective stress in soils, concrete and rocks, in *Pore Pressure and Suction in Soils*, pp. 4-16, Butterworths, London, 1960.

Sleep, N. H., Grain size and chemical controls on the ductile properties of mostly frictional faults at low-temperature hydrothermal conditions, *Pure Appl. Geophys., 143*, 41-60, 1994.

Sleep, N. H., and M. L. Blanpied, Creep, compaction and the weak rheology of major faults, *Nature, 359*, 687-692, 1992.

Sleep, N. H., and M. L. Blanpied, Ductile creep and compaction: a mechanism for transiently increasing fluid pressure in mostly sealed fault zones, *Pure Appl. Geophys., 143*, 10-40, 1994.

Sorby, H. C., On the direct correlation of mechanical and chemical forces, *Proc. R. Soc. London, 12*, 538-550, 1863.

Sorby, H C., On the application of quantitative methods to the study of the structure and history of rocks, *Q. J. Geol. Soc. London, 64*, 171-233, 1908.

Spiers, C. J , P. M. T. M Schutjens, R. H. Brzesowsky, C. J. Peach, J. L. Liezenberg, and H. J. Zwart, Experimental deformation of constitutive parameters governing creep of rock salt by pressure

solution, in *Deformation Mechanisms, Rheology and Tectonics*, edited by R. Knipe, and E. H. Rutter, *Geol. Soc. Spec. Publ., 54*, 215-353, 1990.

Stephenson, L. P., W. J. Plumley, and V. V. Palciauskas, A model for sandstone compaction by grain interpenetration, *J. Sediment. Petrol., 62*, 11-22, 1992.

Tada, R., R. Maliva, and R. Siever, A new mechanism for pressure solution in porous quartzose sandstone, *Geochim Cosmochim Acta, 51*, 2295-2301, 1987.

Takei, Y., Constitutive mechanical relations of solid-liquid composites in terms of grain-boundary contiguity, *J. Geophys. Res., 103*, 18,183-18,203, 1998.

Vigil, G., Z. Xu, S. Steinberg, and J. Israelachvili, Interactions of silica surfaces, *J. Colloid Interface Sci., 165*, 367-385, 1994.

Wahab, A. A., Diagenetic history of Cambrian quartzarenites, Ras Did-Zeit Bay area, Gulf of Suez, eastern desert, Egypt, *Sediment. Geol., 121*, 121-140, 1998.

Wan, Q.-H., Effect of electroosmotic flow on the electrical conductivity of packed capillary columns, *J. Phys. Chem. B, 101*, 4860-4862, 1997.

Watillon, A., and R. de Backer, Potentiel d'écoulement, courant d'écoulement et conductance de surface à l'interface eau-verre, *J. Electroanal. Chem. Interfacial Electrochem., 25*, 181-196, 1970.

Weyl, P. K., Pressure solution and the force of crystallization: A phenomenological theory *J. Geophys. Res., 64*, 2001-2025, 1959.

Yaminski, V. V., B. W. Ninham, and R. M. Pashley, Interaction between surfaces of fused silica in water. Evidence of cold fusion and effects of cold plasma treatment, *Langmuir, 14*, 3223-3235, 1998.

Yang, X. S., Pressure solution in sedimentary basins: effect of temperature gradient, *Earth Planet. Sci. Lett., 176*, 233-243, 2000.

Yates, D. E., and T. W. Healy, The structure of the silica/electrolyte interface, *J. Colloid Interface Sci., 55*, 9-19, 1976.

A. Revil, CNRS-CEREGE, Departement de Géophysique, Europôle Méditerranéen de l'Arbois, BP-80, F-13545 Aix-en-Provence, Cedex 04, France. (revil@cerege.fr)

(Received May 1, 2000; revised November 6, 2000;
accepted December 13, 2000.)